2015

Investigating thermal transport in isotope substituted nanomaterials using molecular simulations

Upamanyu Ray
Iowa State University

Investigating thermal transport in isotope substituted nanomaterials using molecular simulations

by

Upamanyu Ray

A thesis submitted to the graduate faculty

in partial fulfillment of the requirements for the degree of

MASTER OF SCIENCE

Major: Mechanical Engineering

Program of Study Committee:
Ganesh Balasubramanian, Major Professor
Sriram Sundararajan
Krishna Rajan

Iowa State University

Ames, Iowa

2015

DEDICATION

To my family and friends from back in India who have supported and stood by me at every stage of life.

TABLE OF CONTENTS

ACKNOWLEDGEMENTS

I would first like to acknowledge the guidance of my major professor, Dr. Ganesh Balasubramanian for mentoring me and helping me improve as a researcher throughout my stay at Iowa State. I would also like to thank my program of study committee, Dr. Sriram Sundararajan and Dr. Krishna Rajan, for their suggestions and teaching me how to engage in collaborative research.

Secondly, I want to thank my research group for their inputs at opportune moments, which helped me solve many intricate problems. A very special thanks to the Graduate Office of ME that includes Deb, Amy and Neely for their timely assistance in almost everything I needed as a graduate student.

I want to say to my friends from back in India that each one of you will always have a very special place in my heart and you all know that. I will not name anyone as I don't want to miss any names but you mean a lot to me. You keep me waiting for December every year.

Lastly, the contribution from my family is something for which I will always be indebted to them. I need their love and support at every stage of life.

ABSTRACT

Recent research related to carbon nanotubes, graphene and graphene analogous low-dimensional materials (Silicene, MoS_2, WS_2) have sparked tremendous interests in nanoscale sciences due to their promising applications associated with thermoelectrics and electronics. Heat conduction in these nanomaterials occurs by lattice vibration where energy is transmitted by interaction with neighboring atoms in a spring-like oscillating motion. As a result, quantized lattice vibrational elastic waves called phonons are emitted, which are the main contributors to heat conduction in these non-metallic nanomaterials. In analogous two-dimensional (2D) nanomaterials like graphene and silicene, thermal transport is mainly governed by three acoustic phonon modes (lattice vibration): in-plane longitudinal modes, in-plane transverse modes and out-of-plane vibrational modes. However, in carbon nanotubes there are four phonon modes contributing to the heat transport: longitudinal acoustic modes corresponding to the motion of atoms along the axis of the tube, two transverse degenerate modes and a twist mode. Out of all these modes, generally the low frequency, long-range modes are the ones which exert a dominant contribution towards heat transfer whereas high frequency, short-range modes have a very limited contribution to the thermal transport process. Literature contains inconsistent results identifying the dominant vibrational modes for these nanomaterials. In our research we explore this for carbon nanotubes, graphene and silicene. A clear understanding of the transport mechanism can enable design of novel nanomaterials that can be successfully used for targeted applications in thermal management. We have considered nanomaterials with varying dimensions and shape (carbon nanotube and

graphene) and also nanostructures with varying isotope substitution but similar geometries (graphene and silicene).

Using classical molecular dynamics simulations, we identify the delocalized transverse modes in carbon nanotubes and out-of-plane flexural modes in graphene as the dominant modes which contribute mostly to the thermal transport in them. We extend our investigation to analogous 2D materials, graphene and silicene. Even though they are structurally similar, their heat conduction mechanisms are found to vary drastically. In contrast to the dominant out-of-plane flexural modes in graphene, the heat conduction in silicene occurs predominantly due to in-plane transverse acoustic modes. Due to the buckled silicene structure, coupling of the out-of-plane flexural modes and in-plane longitudinal modes causes a mode softening effect. The weaker Si-Si bond strength implies low group velocity of the out-of-plane phonons making them essentially non-existent for silicene. But despite the differences in the phonon modes, the variation in k with increasing isotope substitution in both graphene and silicene are found to be similar. The shift in vibrational spectra towards lower frequencies indicating the reduced energy carrying capacity of phonons due to mass disorder is found to be consistent in silicene too. Our results showing decrease in k in graphene and silicene compared well with an analytical model based on mean-field approximation. We hope that our study will initiate many more fascinating researches in this rapidly evolving area.

CHAPTER 1. GENERAL INTRODUCTION

Nanoscale Heat Transfer

My main inspiration for this thesis came from Noble laureate physicist Richard Feynman's visionary lecture in 1959 titled "There is plenty of room at the bottom" (Feynman. (1959)) where he talks about the possibilities of shrinking the whole world into a piece of dust. Truly, with the advent of microelectromechanical (MEMS) technologies, we have come to realize the veracity of his statements in the 21st century after observing the tremendous level of sophistication achieved in field of experimental and theoretical nanoscale heat transfer.

The influence of the physical size of the system under study in heat transfer has been of prime interest to scientists for over the last two centuries. The involvement of size effects in situations like the interaction with surface boundaries during heat conduction in solids, the fluid layer adjacent to the surface under consideration during convection and electromagnetic heat transport mechanism in radiation heat transfer are immense. This problem becomes more acute when we are dealing with micro or nanoscale systems. Fundamental relations like Fourier's law of heat conduction which are implemented to describe heat transfer at the macroscopic level often become inappropriate for the thermal transport analysis at these small-length-scales. So this calls for a more fundamental bottoms-up approach which combines the salient details of the nanoscale and uses it for accurate predictions at the continuum for utilization of mankind. The stark difference of surface to volume ratio in the

nanoscale level from that of the continuum is also a reason for trying to understand the heat transport phenomenon from a fundamental perspective.

The way atoms, the elementary forms of matter in a system, interact decides its phase (solid/liquid/gas). In solids, the atoms vibrate around an equilibrium position in a closed arrangement but do not move from its place making their relative positions in the structure fixed. In liquids, the atoms are well separated due to weak interaction forces in between whereas in gas, the atoms are in a random arrangement which allows it to move freely. In this study heat conduction of carbon nanotubes, graphene and silicene are dealt with all of which are mostly non-metallic solids. So the significant transport mechanisms that may arise in phases other than the solid are not accounted for.

Heat conduction can occur in two ways namely particle collision and/or lattice vibration. In solids, collision of molecules causes thermal energy to be transferred from one molecule to another. For metals, the atoms are bound to each other causing lattice vibration and at the same time the presence of free electrons is responsible for causing the particle collisions. Metals are much better thermal conductors than non-metals because the same mobile electrons that participate in electrical conduction also take part in the transfer of heat. But in non-metallic solids (like nanotubes and graphenes), the atoms or molecules are bound to each other by a series of bonds acting like springs. The interconnected bonds will form a specific lattice structure. In such a situation, the atom or molecules on the hot side vibrates more vigorously than the atom on the cold side. Heat, in the form of vibration, is transferred to the cold side through a spring-like motion of bonds, a term that is known as lattice vibration. The energy of a given lattice vibration in a rigid crystal lattice is quantized into a phonon. Since in carbon nanotubes, graphene and graphene analogous two dimensional

materials (2-D) like silicene, particle collisions do not occur much due to absence of substantial number of free electrons, the heat conduction primary takes place due to the presence of these phonons. The length scale used for systems at nanoscale dimensions is the mean free path that records the distance between two successive phonon collisions. Ballistic thermal transport occurs when the length of the nanostructure is smaller than the characteristic mean free path. With increase in system dimensions, phonons have a greater likelihood of collision causing a transition to diffusive thermal transport, which exhibits more boundary scattering effects due to reduction in energy losses.

There have been many theoretical and experimental investigations for the study of thermal transport in non-metallic nanomaterials but I have used molecular dynamics simulations, a computational tool derived from classical Newton's equations of motion to model this phenomenon. A detailed picture of the underlying mechanism governing these transport processes will help us develop a consistent framework which can then be implemented to treat the thermal energy transport phenomenon in a macroscale model.

Molecular Dynamics

Molecular dynamics (MD) is a versatile and powerful, deterministic, discrete modelling tool which can provide a sound analysis in the nanoscale domain and measure properties that are impossible to calculate in the laboratory. If we have enough computational power, the trajectories of all the atoms or molecules in a system can be traced which helps us evaluate the macroscale properties of the system and also scrutinize the microscopic processes in progress. When the equations of all the atomic trajectories are coupled by using classical Newton's laws of motions and a suitably chosen expression of interatomic potential

(or force), then those equations can be solved numerically in MD (Chen. (2005)). So this tool is like a computational "experiment" beneficial in saving time and resources that, or else, are incurred during experiments.

Numerical integration of equations of translational motion describes the change in positions, velocities and orientation of molecules in the system over time (Sobhan, Peterson. (2008)). The interaction potential used (U) models the bonded as well as non-bonded attractions and repulsions among the atoms in the real space. The equations of force (F) used are:

$$F = -\frac{\partial U}{\partial r} = \frac{\partial^2 r}{\partial t^2}$$

Numerical integration yields particle velocities and then each particle is moved through a distance equal to the calculated velocity multiplied by the simulation time step (generally in the order of 10^{-12} seconds or 10^{-15} seconds). It is worth noting here that in MD, small time steps are preferred because otherwise, particles in the system may overlap each other increasing the overall energy and causing an unstable regime. In our calculations, the potential used throughout is the three-body Tersoff potential (Tersoff. (1989)) as it has been known to provide robust predictions in the nanomaterials (carbon nanotubes, graphene and silicene) under consideration.

So the basic steps followed while performing MD simulations (Haile. (1997)) are as follows:

1. The simulation box (domain) is defined and the appropriate potential functions are assigned to reproduce the atomic interactions of the nanomaterials used. All the nanostructures are created in this study using the topotool plugin of the Visual Molecular Dynamics (VMD) software.

2. The next step is energy minimization that is mainly geometry optimization and does not involve thermodynamics. Optimization is performed mainly by steepest descent and/or conjugate gradient method.

3. The system is equilibrated by defining an (or many) appropriate ensemble(s) until when the distribution of the "local" states of the individual particles in the system become representative of the "global" states.

4. The forces on the atoms are computed by integrating the equations of motions and the atoms are updated to their new positions.

5. After equilibrating the system, a "production run" is executed where the system evolves over time and the required static and/or dynamic properties are calculated.

For calculations of thermal conductivity (k) in my investigation, a technique called reverse non-equilibrium molecular dynamics (RNEMD) is used which is more explicitly discussed in Chapter 2.

Thesis Organization

The following Chapters 2, 3 and 4 develop more on the outlines of MD discussed above. Specifically, Chapter 2 describes the role of isotope substitution in the thermal conductivity reduction of carbon nanotubes (CNTs) and graphene nanoribbons (GNRs) and the influence of dominant and non-dominant vibrational modes in the energy transport mechanism. Chapter 3 presents a computational framework using informatics to express the thermal conductivity of isotope substituted GNRs as a function of phonon density of states, which will accelerate the prediction of thermal conductivities in absence of the need to use time-consuming MD simulations. Here my contribution was evaluation of the phonon density

of states and preparation of the manuscript. Our collaborators Dr. Scott Broderick, Dr. Srikant Srinivasan and Dr. Krishna Rajan were involved in the informatics based analysis and in the preparation of manuscript. Chapter 4 talks about how, in spite of having similar honeycomb lattice structures, GNR and silicene nanoribbons (SNR) differ in their heat transport mechanism but still keeps the trend of change in thermal conductivity due to isotope substitution intact.

Finally, Chapter 5 summarizes all the conclusions that can be drawn from the thesis and recommends future researches that can be undertaken by defect engineering as means of designing novel carbon and graphene analogous 2-D materials.

The Chapters 2 and 3 are published journal articles and Chapter 4 is intended for archival publication. Appropriate references are added at the end of each chapter. Appendix at the end of the thesis shows the input files used to execute the MD simulations in LAMMPS (Large-scale Atomic/Molecular Massively Parallel Simulator) for the cases of pure and isotope substituted graphene.

References

[Feynman, R.P. (1991) There's Plenty of Room at the Bottom. *Science*. **254**. 1300-1301.]

[Chen, G. (2005) Nanoscale Energy Transport and Conversion. *Oxford University Press*. 452.]

[Sobhan, C.B, Peterson, G.P. (2008) Microscale and Nanoscale Heat Transfer - Fundamentals and Engineering Applications. *CRC Press*. 336]

[Tersoff, J. (1989) Modeling Solid-State Chemistry: Interatomic Potentials for Multicomponent Systems *Phys. Rev. B*. **39**. 5566-5568]

[Haile, J.M. (1997) Molecular Dynamics Simulations - Elementary Methods. A Wiley Interscience Publication. 38-91]

CHAPTER 2. REDUCED THERMAL CONDUCTIVITY OF ISOTOPE SUBSTITUTED CARBON NANOMATERIALS: NANOTUBE VERSUS GRAPHENE NANORIBBONS

Modified from a paper published in *Chemical Physics Letters* 599, 154–158, (2014)

[1]Upamanyu Ray and Ganesh Balasubramanian[*]

Abstract

Non-equilibrium molecular dynamics (MD) simulations of isotopically impure carbon nanotubes (CNTs) and graphene nanoribbons (GNRs) of varying lengths reveal that the relative decrease in thermal conductivity (k) in both the nanostructures are similar for constant isotope substitution. We find that the delocalized transverse modes in CNTs and the out-of-plane flexural modes in GNRs exert a substantial contribution to the thermal transport whereas the influence of isotope substitution on the phonon density of states (DOS) is similar in all directions. The vibrational spectra for different length scales consistently show that the energy modes shift to lower wave numbers reflecting the strong influence of mass disorder that reduces the energy transport through these nanomaterials, consequently lowering k.

[1]Department of Mechanical Engineering, Iowa State University, Ames, IA 50011, USA

*Corresponding author. Email:bganesh@iastate.edu

1. Introduction

Carbon nanomaterials have received widespread interest since their discovery [1] because of their unique mechanical, thermal and electrical properties. However, ambiguity exists about the differences in the fundamental physics governing heat transfer through 1D (or semi-1D as some previous literature [2,3] suggest but since that does not influence our analysis, we refer to carbon nanotubes or CNTs as a 1D material throughout) and 2D (graphene nanoribbons or GNRs) [4,5] forms of carbon nanomaterials. For instance, there is disagreement in the literature about the dominant phonon (lattice vibration) modes that contribute to the thermal transport through them [6,7]. This could become more significant in presence of mass disorder created by isotope or vacancy defects in these nanomaterials which have been observed from theoretical as well as experimental studies in these nanomaterials [8–11]. Thus, comparing the heat conduction mechanisms in CNTs and GNRs [12,13] would facilitate design of novel carbon nanomaterials and prediction of their transport characteristics geared towards targeted applications in electronics, thermoelectrics etc [14–18].

Earlier investigations [6] suggest that for graphene the in-plane vibrational modes along the direction of heat transfer mainly influence the thermal transport while other efforts propose that the out-of plane low energy flexural vibrational modes exert the dominant effect on the heat transfer. Here, we employ classical molecular simulations to explore contributions of the various vibrational modes in the heat transfer through these carbon nanostructures, with and without isotope substitution. Our study provides insinuations about the decrease in k with mass disorder induced by the presence of isotopes and investigates whether mass impurities influence the dominant or non-dominant modes or both, causing impedance to heat transfer.

Reports that describe the role of isotope substitution on thermal conductivity for varying material dimensions are sparse. We present our findings for reduction in *k* with constant isotope (^{14}C) substitution in both CNT and GNR with varying material lengths, and infer that the relative thermal conductivity decrease for isotope substituted nanomaterials relative to the pure forms remains invariant to changes in the characteristic dimension. The contribution of the mass disorder to both the dominant and the non-dominant vibrational modes are described.

2. Methodology

We employ MD simulations to examine armchair (10, 10) CNTs and GNRs with lengths (*x*-direction) ranging from 20-110nm with varying number of carbon atoms, as listed in Table 1. As the literature[19,20] suggests that *k* is strongly dependent on the thickness of GNRs and the diameter and chirality of CNTs, these parameters are kept invariant in our investigations. The CNTs are made by zone-folding approach from GNRs of similar lengths and 4.26nm width (*y*-direction). The thickness of the GNR sheet is the van der Waals diameter of a carbon atom, 0.34 nm [21]. We select 10% of the carbon (^{12}C) atoms randomly and substitute them by the heavier ^{14}C isotope. Each structure is initialized at a temperature of 300 K and pressure of approximately 1 bar. Periodic boundary conditions (PBCs) are imposed in all directions with the *y*- and *z*-axes dimensions of the simulation cell large enough to prevent the structures from interacting with their own periodic images. We employ the 3-body Tersoff potential that models the attractive and repulsive bonded as well as the non-bonded interactions in both CNTs and GNRs, and is known to provide robust predictions [22–26]. The highly parallelized LAMMPS package [27] is used for all our simulations.

Table 1. The length (*L*) of the nanostructures (CNT and GNR) and number of carbon atoms contained in them are listed. The corresponding simulation box dimensions are L(*x*) × 4.26 nm(*y*) × 10.4 nm(*z*) for GNRs and L(*x*) × 10.4 nm(*y*) × 10.4 nm(*z*) for CNTs. The numbers of atoms involved in the energy exchange for thermal conductivity calculations are also listed.

Length of GNRs/CNTs (nm)	20	35	50	65	80	95	110
Number of atoms	3280	5720	8160	10600	13040	14680	17920
Total number of atoms in the two cold slabs at the nanomaterial boundaries	66	120	160	240	253	330	360
Total number of atoms in the hot slab at the center of the nanomaterial	66	120	160	240	253	330	360

We perform equilibrium MD simulations with isothermal-isobaric ensemble (NPT) under the Nóse-Hoover thermostat and barostat (each with a coupling time of 0.1 picosecond (ps)) followed by canonical (NVT) simulations, each for 7 nanoseconds (ns). Subsequently, simulations under the microcanonical ensemble (NVE) are employed for a further 2 ns to equilibrate the system in absence of imposed constraints. A timestep of 0.001 ps is used throughout in all the simulations. The results are obtained under the ergodic hypothesis assumption employing a time average for the computed data in lieu of an ensemble sampling

[28]. We calculate the phonon density of states (DOS) from the Fourier transform of the averaged mass-weighted velocity autocorrelation function (VACF). We continue the equilibrium simulations for additional 1 ns recording the trajectories of the equilibrated nanostructures after every 100 ps. Each of these are again simulated for an additional 8.5ps where the velocities, recorded after every 1 fs, are used to compute the time-translation invariance of the VACF with a correlation time of 8.192 ps and averaging over 309 time origins. The overall average of all the VACFs is Fourier transformed to obtain the desired phonon DOS spectra with a resolution of 2.036 cm^{-1}. The heat transfer is along the *x*-wise direction for both CNTs and GNRs. For the nanotubes both *y*- and *z*- axes are the transverse directions, while the *z*-axis represents the out-of-plane direction for the 2D GNRs.

We apply the reverse non-equilibrium MD (RNEMD [29,30] approach to compute the thermal conductivities for the different GNRs and CNTs along the in-plane *x* direction using the canonical (NVT) ensemble for 8 ns. Each of the structures are partitioned into 100 bins (or "slabs") along the *x*-direction. In the present research, the number of slabs is constant for all lengths of the nanomaterials and equal to 100. Hence the size of each slab increases with increasing lengths of the nanostructures and the number of atoms involved in the energy exchange process is provided in Table 1. Employing a kinetic energy exchange mechanism, the central bins are artificially heated while the ones at the boundaries are cooled. Around 280 atoms from the cool boundaries and the same number from the hot slab at the center get involved in this energy exchange. This drives a heat transfer process through the nanomaterial. A steady state temperature distribution is achieved after 7 ns which is used to calculate the heat flux through the material and the temperature gradient. We continue the simulations for additional 1 ns to compute the average energy transferred and the spatially

distributed temperature values. Figures 1(a) and (b) respectively show the spatial temperature distribution for pure CNT and GNR of length 50 nm. We find the temperature distributions are linear and symmetric about the mid-plane of the nanostructures [21,30]. Given the linear variation of temperature, we employ the empirical Fourier's Law to compute k. We obtain $k = [\sum(m/2)(V_h^2 - V_c^2)] /(2t\ A_{xy}\ dT/dx)$, where $\sum(m/2)(V_h^2 - V_c^2)$ provides the kinetic energy exchanged within the simulated structure, t is the simulation time, A_{xy} is the cross-sectional area across which heat transfer occurs and dT/dx is the temperature gradient. Disagreements exist in the determination of the cross-section, especially for CNTs [31–33]. We use the Van der Waals diameter of each carbon atom as the thickness of the nanotube or nanoribbbon throughout our analysis. For nanotube the cross-sectional area is that of a concentric cylinder with its thickness being the diameter of a carbon atom. On the other hand, for the nanoribbons, the cross-section is simply the rectangular area with the width (y-axis) of GNR (4.26nm) and thickness equal to the diameter of the carbon atom.

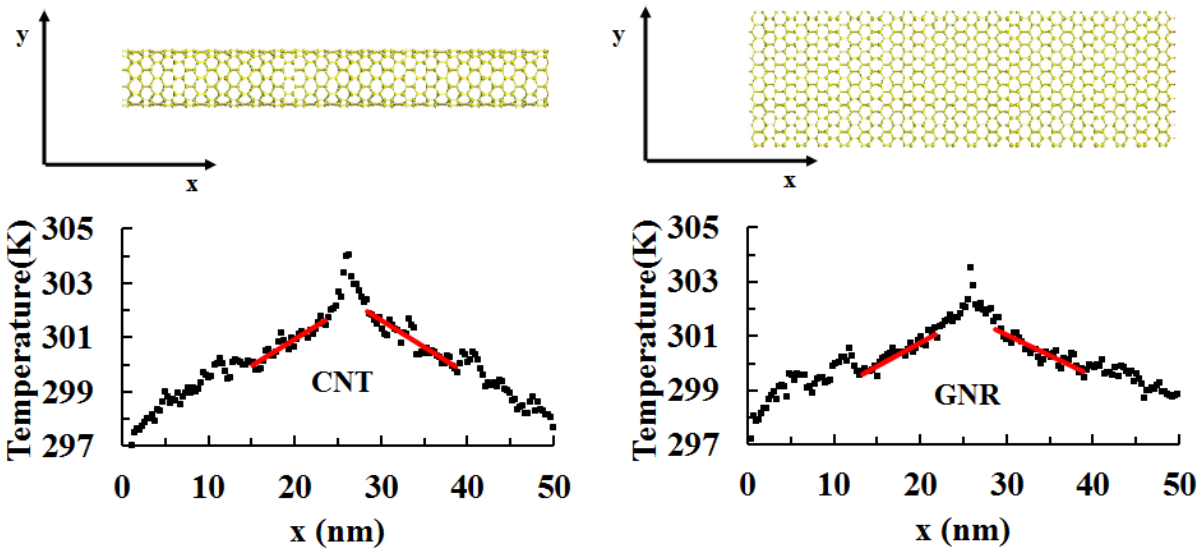

(a) **(b)**

Figure 1: The steady-state temperature distribution along the direction of heat transfer obtained from the MD simulations are presented for (a) CNT and (b) GNR, each of length *L* = 50 nm.

3. Results and Discussion

The length dependence of *k* for both pure and isotopically impure CNTs and GNRs are presented in Figures 2(a) and (b).*k* varies from 101.2725 $Wm^{-1}K^{-1}$ for 20 nm pure CNT to 345.706 $Wm^{-1}K^{-1}$ for 110 nm pure CNT while the corresponding pure GNRs have *k* = 86.34 $Wm^{-1}K^{-1}$ and 215.5 $Wm^{-1}K^{-1}$ respectively. The increase in *k* with increasing length agrees well with earlier computational investigations [21,34,35]. Minor differences in the numerical results arise due to the interatomic potential functions employed for the atomistic simulations [36,37]. Our results reveal ~32% decrease in *k* when GNRs are 10% isotope substituted with ^{14}C, and compare well with earlier experiments that show ~35% decrease in *k* when a pure

GNR is isotope substituted with ^{13}C [10]. *k* varies linearly with length of the nanostructures. Thermal transport is ballistic when nanostructure length is smaller than the characteristic mean free path and the energy scattering due to inelastic phonon-phonon collisions are negligible. As the system size increases, phonons have a greater likelihood of colliding with one another resulting in a transition to diffusive transport. Increase in dimension reduces the energy losses due to boundary scattering resulting in an effectively higher *k* [38–41].

Isotope substituted nanostructures, as expected, have lower *k* than their pure counterparts because the presence of mass impurities creates hindrance to the formation of delocalized modes impeding thermal transport [42]. Characteristic vibrational modes for the different isotopes contribute to enhanced interactions between phonons at different frequencies facilitating increased energy scattering. *k* variation with length for the pure and 10% isotope substituted samples are linear and almost parallel to each other for both for CNTs and GNRs. The ratio of the spatial gradients of the pure and isotope substituted *k*-plots are approximately equal (~0.84) for both the nanomaterials. We corroborate that for a given concentration of isotopes, the relative rate of change of *k* with increasing system dimension is similar for both the CNT and the GNR. Hence, the influence of mass disorder on thermal transport through carbon nanomaterials is independent of the dimensionality of the nanostructure. Figure 2(a) and (b) also show a non-linearity in the variation of $1/k$ with large *L*. This is the region where transition from ballistic to diffusive regime occurs and the linear correlation between *k* and *L* is not appropriate.

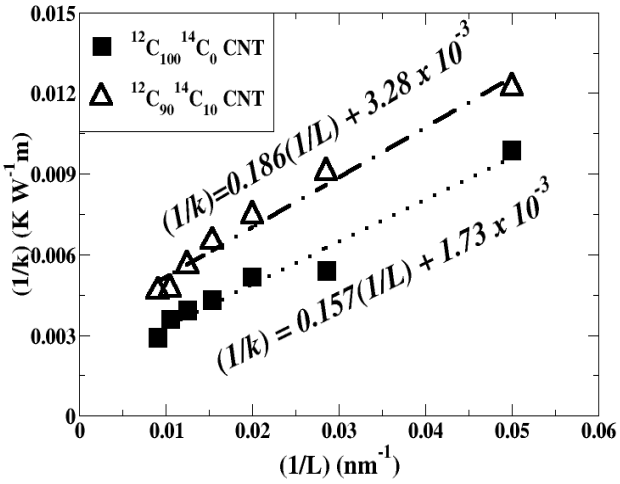

(a)

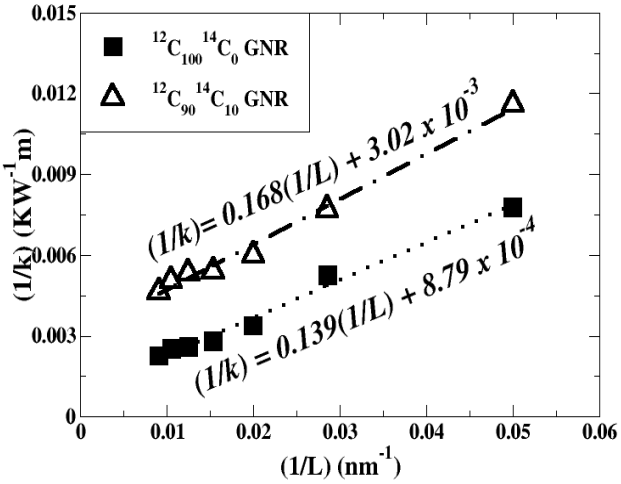

(b)

Figure 2. The variation of 1/*k* with 1/*L* for both pure and 10% isotope substituted (a) CNTs and (b) GNRs of lengths *L* = 20 nm, 35 nm, 50 nm, 65 nm, 80 nm, 95 nm & 110 nm are presented. The fitting curves shown as dashed lines represent the linear inter-relationship between *k* and *L* for both pure and isotope substituted nanomaterials.

In order to explore the contribution of isotope substitution to the different vibrational modes influencing heat transfer in CNTs and GNRs, we investigate the phonon DOS. In GNR, 6 characteristic vibrational modes [43–45] can be identified of which 3 are acoustic: an in-plane transverse mode (*y*-wise), an in-plane longitudinal mode (*x*-wise) and an out-of-plane flexural mode (*z*-direction) [46]. The remaining are optical modes that have negligible contribution to the thermal transport [47]. Rolling a graphene sheet into a CNT affects the phonon dispersion by collapsing the 2D band structure of the GNR to one-dimensional discrete sub-bands [43]. The four phonon modes that potentially contribute to thermal transport across a CNT are the longitudinal acoustic (LA) mode corresponding to the motion of atoms along the tube axis, two degenerate transverse acoustic modes (TA) corresponding to the atomic displacements perpendicular to the nanotube axis and a twist mode corresponding to the torsion of the tube around its axis. The acoustic modes in the longitudinal direction for both GNR and CNT are effectively the same.

We compute the phonon DOS for various lengths (20nm, 35nm, 50nm, 65nm, 80nm, 95nm and 110nm) of both the nanostructures under consideration. Amongst them, results corresponding to the 50nm CNTs and GNRs are presented in Figure 3 since the other structures follow similar trends. From Figure 3(b), we observe that the low wave number delocalized transverse modes occur around 310 cm^{-1} and 620 cm^{-1} for pure CNTs which agrees well with previous investigations [48]. Thus these delocalized vibrational modes also exert a substantial contribution to heat transfer [36,40]. On the other hand, the longitudinal modes at higher wave numbers, shown in Figure 3(a), correspond to the high energy short-ranged stretching modes of carbon atoms about their equilibrium position. The peaks occurring at around 1300 cm^{-1} and 2100 cm^{-1} for the modes along the *x*-direction of the 50nm

CNT are localized. Substituting 10% of ^{12}C atoms by their ^{14}C isotope shifts the peaks of the vibrational modes along both the longitudinal and transverse directions towards lower wave numbers [49], as illustrated through the magnified sections of Figures 3(a) and (b). Although this shift is more conspicuous in the higher wave number region and less prominent in the lower frequency domain, transition of the vibrations to lower wave numbers implies that the mass disorder reduces the energy carrying capacity of the phonons.

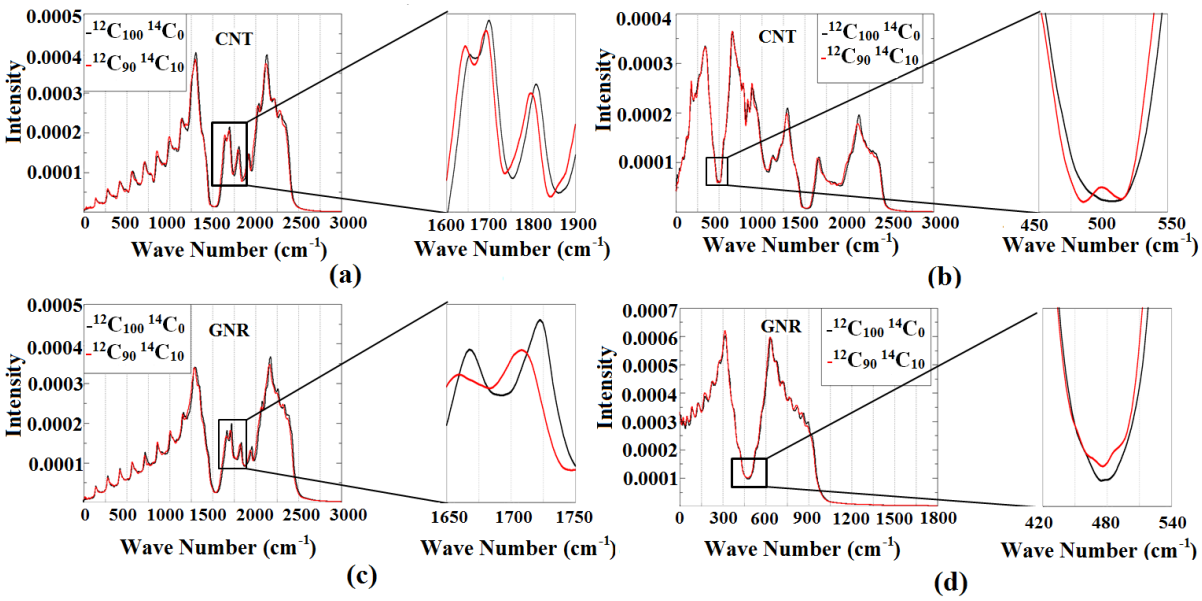

Figure 3: The phonon DOS for pure (black) and 10% isotope substituted (red) nanomaterials of length *L* = 50 nm are presented for both along the direction of heat transfer (*x*) [(a) for CNTs and (c) for GNRs] and perpendicular to it (*z*) [(b) for CNTs and (d) for GNRs]. The intensity of the DOS is given in arbitrary units. Sections of the DOS are magnified to illustrate the shift in the phonon spectra to lower wave numbers for isotope substituted nanomaterials.

Similar effects are observed from the DOS of 50 nm long GNR as shown in Figures 3(c) and (d). The peaks of low energy out-of plane (*z*-direction) vibrational modes for the pure nanoribbon are observed at around 310 cm^{-1} and 630 cm^{-1} as presented in Figure 3(d). They correspond to the flexural vibrational modes of GNR perpendicular to the direction of heat transfer and contribute to the heat conduction substantially [50], although their dominance in the heat transfer process is debatable. The high energy localized vibrational modes, along the in-plane (*x*- or *y*- directions), as shown in Figure 3(c), having peaks at 1300 cm^{-1} and 2100 cm^{-1} comparatively exert lesser contribution to the thermal transport. Although counterintuitive, the out-of-plane vibrational modes propagate farther than their in-plane counterparts, resulting in a stronger contribution to energy transport through the delocalized phonons. The in-plane vibrations at higher frequencies mimic short-ranged stretching modes and have a relatively lower contribution to the heat transfer across the plane of the GNR. Similar to the CNTs, the vibrational spectra of the isotope substituted GNRs shows a shift to lower wave numbers that contributes to its reduced energy carrying capacity. It is important to note that for both the nanostructures, isotope substitution affects the dominant as well as the non-dominant lattice vibrations, irrespective of the dimensionality of the nanomaterial.

The total phonon DOS for 20 nm and 110 nm lengths of isotope substituted CNTs and GNRs are compared in Figures 4(a) and (b) respectively. From Figure 4(a), we find that the spectra of low frequency delocalized transverse vibrational modes and the localized vibrational modes at higher wave numbers for both the lengths of CNTs are exactly the same implying that even for different lengths of the nanotubes, effect of mass disorder is similar in reducing in energy carrying capacity of phonons. Likewise, we obtain similar results for the changes in

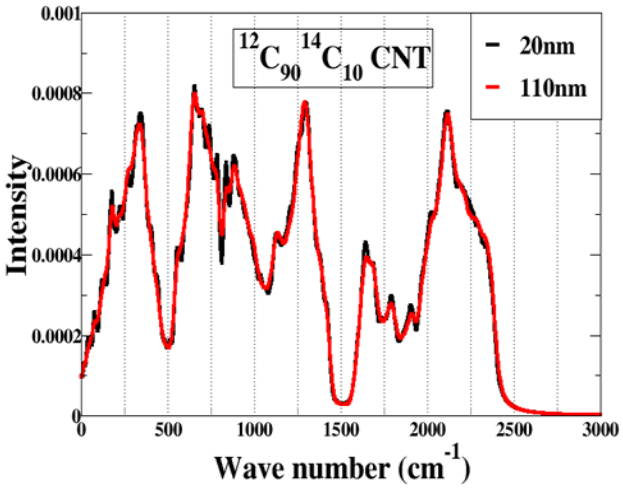

(a)

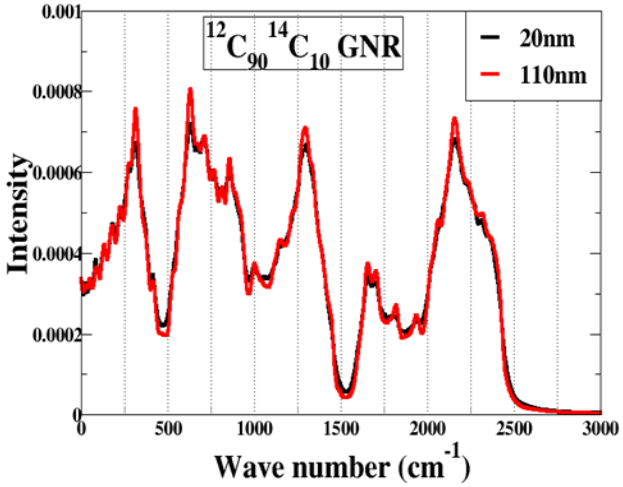

(b)

Figure 4: The phonon DOS for both isotope substituted (a) CNTs and (b) GNRs of different lengths *L* = 20 nm (black) and 110 nm (red) are shown. The intensity of the phonon spectra are in arbitrary units.

the flexural modes and in-plane lattice vibrations for GNRs of different dimensions, as shown in Figure 4 (b). The influence of mass disorder in shifting the vibrational spectra is consistent across different material lengths.

4. Conclusion

In summary, our atomistic simulations predict the decrease in thermal conductivity of isotope substituted 1D and 2D carbon nanomaterials. The relative decrease in thermal conductivity for a constant percentage of isotope substitution in CNTs and GNRs of equivalent lengths is similar for the whole length scale leaving the ballistic-diffusive regime. The induced mass disorder shifts the vibrational spectra to lower wave numbers. This is observed for both the acoustic flexural out-of-plane modes in GNR and the low frequency delocalized transverse modes in CNTs as well as the short-ranged longitudinal modes in CNT and in-plane vibrations in GNR thus influencing thermal transport. Contribution of isotope substitution to the thermal conductivity is consistent over a range of material lengths for both the nanostructures.

Acknowledgments

We thank the Extreme Science and Engineering Discovery Environment (XSEDE), which is supported by National Science Foundation grant number OCI-1053575, for use of the computing clusters Lonestar and Stampede.

References

[1] S. Iijima, Nature. 354 (1991) 56–58.

[2] M. Alaghemandi, F. Leroy, E. Algaer, M.C. Böhm, F. Müller-Plathe, Nanotechnology. 21 (2010) 75704.

[3] M. Alaghemandi, F. Leroy, F. Müller-Plathe, M.C. Böhm, Phys. Rev. B. 81 (2010) 125410.

[4] K. S. Novoselov, V. I. Fal'ko, L. Colombo, P. R. Gellert, M. G. Schwab, Nature. 490 (2012) 192–200.

[5] E. Pop, V. Varshney, A. K. Roy, MRS Bull. 37 (2012) 1273–1281.

[6] J. Turney, E. Landry, A. McGaughey, C. Amon, Phys. Rev. B. 79 (2009) 064301.

[7] D. Donadio, G. Galli, Phys. Rev. Lett. 99 (2007) 255502.

[8] G. Zhang, B. Li, Nanoscale. 2 (2010) 1057.

[9] F. Hao, D. Fang, Z. Xu, Appl. Phys. Lett. 99 (2011) 041901.

[10] S. Chen, Q. Wu, C. Mishra, J. Kang, H. Zhang, K. Cho, et al., Nat. Mater. 11 (2012) 203–207.

[11] C. Sevik, G. Cuniberti, Nano Lett. 11 (2011) 4971–4977.

[12] A. A. Balandin, D. L. Nika, Mater. Today. 12 (2012) 266.

[13] K. M. F. Shahil, A. A. Balandin, Solid State Commun. 152 (2012) 1331–1340.

[14] S. Stankovich, D. A. Dikin, G. H. B. Dommett, K. M. Kohlhaas, E. J. Zimney, E. A. Stach et al., Nature. 442 (2006) 282–286.

[15] F. Scarpa, S. Adhikari, A. Srikantha Phani, Nanotechnology. 20 (2009) 065709.

[16] R. Sengupta, M. Bhattacharya, S. Bandyopadhyay, A. K. Bhowmick, Prog. Polym. Sci. 36 (2011) 638–670.

[17] M. Terrones, A. R. Botello-Méndez, J. Campos-Delgado, F. López-Urías, Y. I. Vega-Cantú, F. J. Rodríguez-Macías et al., Nano Today. 5 (2010) 351–372.

[18] M. F. L. De Volder, S. H. Tawfick, R. H. Baughman, A. J. Hart, Science. 339 (2013) 535–539.

[19] T. Falat, B. Platek, J. Felba, 11th Electron. Packag. Technol. Conf. (2009) 636–639.

[20] J. Wang, J. S. Wang, Appl. Phys. Lett. 88 (2005) 4–7.

[21] M. Alaghemandi, E. Algaer, M. C. Böhm, F. Müller-Plathe, Nanotechnology. 20 (2009) 115704.

[22] J. Tersoff, Phys. Rev. B. 39 (1989) 5566-5568.

[23] L. Lindsay, D. A. Broido, Phys. Rev. B. 81 (2010) 205441.

[24] R. Khare, S. Mielke, J. Paci, S. Zhang, R. Ballarini, G. Schatz et al., Phys. Rev. B. 75 (2007) 075412.

[25] J. W. Jiang, J. S. Wang, B. Li, Phys. Rev. B. 81 (2010) 073405.

[26] V. Tewary, B. Yang, Phys. Rev. B. 79 (2009) 075442.

[27] S. Plimpton, J. Comput. Phys. 117 (1995) 1–19.

[28] J. Wang, P. Wolynes, Phys. Rev. Lett. 74 (1995) 4317–4320.

[29] F. Müller-Plathe, J. Chem. Phys. 106 (1997) 6082.

[30] J. Park, M. F. P. Bifano, V. Prakash, J. Appl. Phys. 113 (2013) 034312.

[31] J. Chen, G. Zhang, B. Li, J. Chem. Phys. 135 (2011) 204705.

[32] A. Peigney, C. Laurent, E. Flahaut, R. R. Bacsa, A. Rousset, Carbon. 39 (2001) 507–514.

[33] S. Chakraborty, J. Chattopadhyay, H. Peng, Z. Chen, A. Mukherjee, R. S. Arvidson et al., J. Phys. Chem. B. 110 (2006) 24812–24815.

[34] W. A. G. III, J. Che, T. Çağin, Nanotechnology. 11 (2000) 65–69.

[35] J. R. Lukes, H. Zhong, J. Heat Transfer. 129 (2007) 705.

[36] J. W. Lee, A. J. Meade, E. V. Barrera, J. A. Templeton, Proc. Inst. Mech. Eng. Part N J. Nanoeng. Nanosyst. 224 (2010) 41–54.

[37] X. Li, J. Chen, C. Yu, G. Zhang, Appl. Phys. Lett. 103 (2013) 013111.

[38] L. Lindsay, D. Broido, N. Mingo, Phys. Rev. B. 80 (2009) 125407.

[39] J. Shiomi, S. Maruyama, Jpn. J. Appl. Phys. 47 (2008) 2005–2009.

[40] M. H. Bae, Z. Li, Z. Aksamija, P. N. Martin, F. Xiong, Z. Y. Ong et al., Nat. Commun. 4 (2013) 1734.

[41] A. Cao, J. Qu, J. Appl. Phys. 112 (2012) 013503.

[42] G. Balasubramanian, I. K. Puri, M. C. Böhm, F. Leroy, Nanoscale. 3 (2011) 3714–20.

[43] J. Hone, Appl. Phys. 80 (2001) 273–286.

[44] M.S. Dresselhaus, G. Dresselhaus, R. Saito, Carbon. 33 (1995) 883–891.

[45] J. Hone, Dekker Encycl. Nanosci. Nanotechnol. (2004) 603–611.

[46] D. L. Nika, E. P. Pokatilov, A. A. Balandin, Phys. Status Solidi. 248 (2011) 2609–2614.

[47] D. L. Nika, A. A. Balandin, J. Phys. Condens. Matter. 24 (2012) 233203.

[48] D. Donadio, G. Galli, Phys. Rev. Lett. 102 (2009) 195901.

[49] A. Sgouros, M. M. Sigalas, G. Kalosakas, K. Papagelis, N. I. Papanicolaou, J. Appl. Phys. 112 (2012) 094307.

[50] L. Lindsay, D. A. Broido, N. Mingo, Phys. Rev. B. 82 (2010) 115427.

CHAPTER 3. AN INFORMATICS BASED ANALYSIS OF THE IMPACT OF ISOTOPE SUBSTITUTION ON PHONON MODES IN GRAPHENE

Modified from a paper published in *Applied Physics Letters* 104, 243110, (2014)

Scott Broderick[1], Upamanyu Ray[2,*], Srikant Srinivasan[1], Krishna Rajan[1] and Ganesh Balasubramanian[2,Ψ]

Abstract

It is shown by informatics that the high frequency short ranged modes exert a significant influence in impeding thermal transport through isotope substituted graphene nanoribbons (GNR). Using eigenvalue decomposition methods, we have extracted features in the phonon density of states (DOS) spectra that reveal correlations between isotope substitution and phonon modes. This study also provides a data driven computational framework for the linking of materials chemistry and transport properties in 2D systems.

[1]Department of Material Science and Engineering

[2]Department of Mechanical Engineering, Iowa State University, Ames, IA 50011

[Ψ] Corresponding author: 2092 Black Engineering Building, Iowa State University, Ames, IA 50011, Phone 515-294-9226, Email: bganesh@iastate.edu

*Contribution included evaluation of the phonon density of states and preparation of the manuscript.

2D materials are increasingly gaining attention from the scientific community due to their remarkable transport properties.[1–6] This started with the groundbreaking discovery of graphene and its notable thermal and electrical properties. Designing novel 2D materials that offer targeted transport properties requires a thorough understanding of the fundamental physics that governs the material behavior. One area of interest over the recent past has been reduction of thermal conductivity of graphene and other carbon nanomaterials through defect engineering for potential thermoelectric applications[7] as well as in high frequency analog circuits and sensors.[8,9] While structural defects can be engineered into the carbon nanomaterial by external means,[10] naturally occurring point defects in graphene can be realized from presence of isotopes or atomic vacancies that induce mass disorder in the nanostructure.[11,12]

In isotope substituted graphene nanoribbons, mass disorder enhances phonon scattering thereby reducing thermal conductivity.[11,12] Both the in-plane and out-of plane vibrational modes are influenced by isotope substitution. In spite of the earlier theoretical investigations, there exists a knowledge gap when correlating the thermal conductivity to the characteristics of phonons in isotope substituted graphene. A qualitative and quantitative connection between the vibrational characteristics of the nanomaterials[13] and its transport properties is extremely important not only to (i) understand the interrelationship between the underlying fundamental physics and the transport phenomenon, but also to (ii) construct design paradigms to engineer new material chemistries at the atomic level that offer desired properties for targeted applications.[14] In this letter, by employing a data driven material informatics technique we reveal that for mass disordered graphene nanoribbons the short ranged high frequency vibrational modes exert a significant contribution towards reducing

the thermal conductivity along the plane of the nanostructure and propose a methodology for accelerated prediction of their thermal conductivities.

We employ classical molecular dynamics (MD) simulations to examine 50 nm (x) × 4.26 nm (y) graphene nanoribbons contained in a simulation box of 50 nm × 4.26 nm × 10.4 nm with periodic boundary conditions in all directions. The highly parallelized LAMMPS code[15] is employed for the MD simulations. The z dimension of the simulation cell is large enough to ensure that the carbon atoms do not interact with their own periodic images in the out-of-plane direction. Various percentages (10, 25, 35, 50, 60, 75, 90 and 100%) of the 8160 ^{12}C atoms are randomly selected and substituted with the heavier ^{14}C isotopes. Each system is initialized at 300K and 0.1 MPa. The 3-body Tersoff potential,[16,17] which is known to provide reasonably accurate representation of transport physics in graphene, is used to describe the different interatomic interactions. Equilibrium MD simulations under the isothermal-isobaric ensemble (NPT) using the Nóse-Hoover thermostat and barostat with coupling times of 0.1 picosecond (ps), followed by canonical (NVT) simulations, each for 7 nanoseconds (ns), are performed in order to release the internal stresses and equilibrate the system. Subsequently, simulations using the microcanonical ensemble are run for a further 2 ns to ensure the nanostructure is equilibrated in absence of external constraints. A timestep of 0.001 ps is used throughout for all the simulations. While performing the equilibrium simulations we dump the atom trajectories after every 50000 timesteps and find the structure to be stable by visualizing it in the Visual Molecular Dynamics (VMD) software[18]. We perform equilibrium simulations[19] for an additional 1 ns and trajectories of the nanoribbon atoms are sampled every 100 ps. Each of these are separately simulated for additional 8.5 ps when velocities of all the atoms are recorded after every 0.001 ps, all of which are used to

compute the time-translation invariance of the mass-weighted velocity autocorrelation function (VACF) with a correlation time of 8.192 ps[19] and averaging over 309 time origins. The phonon DOS spectra with a 2.036 cm^{-1} resolution is calculated from the Fourier transform of the average of all the VACFs.[20,21] The DOS in the in-plane (*x*- or *y*-) and out-of plane (*z*-) directions are computed.

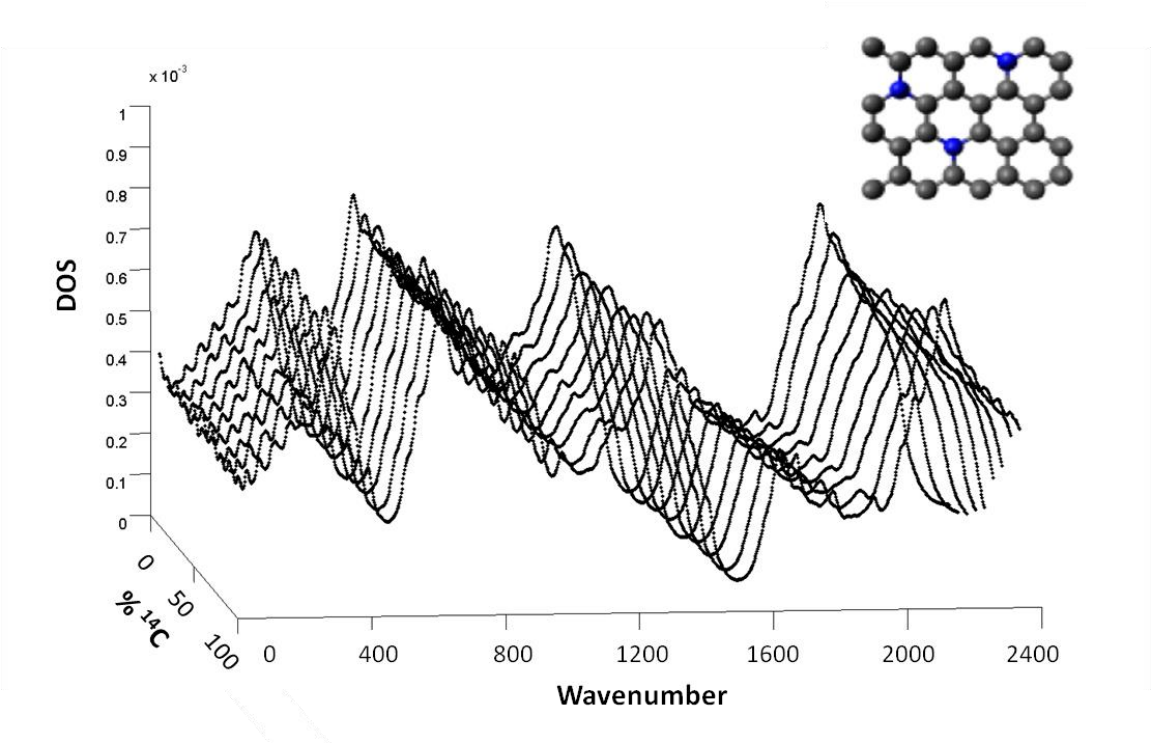

Figure 5. Input phonon DOS into the informatics analysis. The total DOS curves represent the vibrational modes associated with GNR containing different ratios of ^{12}C and ^{14}C. The isotope substitution is structurally represented in the graphene sheet shown in the inset, where the blue atoms represent ^{14}C isotopes. The thermal conductivity of these materials is known to decrease till ^{14}C percentage reaches 50% and then increases with increasing fraction of the heavier isotope.[11,12] Trends in the DOS that correlate quantitatively to this phenomenon are not readily identifiable from the spectra, thus requiring the use of informatics and eliminate the need for extensive computations or measurements.

The total phonon DOS spectra for graphene nanoribbons, presented in Fig. 5, reveals the vibrational characteristics of the different modes in representative ^{14}C isotope substituted structures. The phonon modes that are delocalized are expected to have the dominant contribution in heat conduction through graphene.[11,12] Earlier investigations[22] predict vibrational modes below 800 cm^{-1} to be delocalized to a large extent while higher wavenumbers correspond to localized stretching modes of carbon atoms about their equilibrium position. Along the plane of the pure ^{12}C graphene nanoribbon, the peak observed at 1350 cm^{-1} corresponds to the fastest vibrational modes in the material. On the other hand, the peaks occurring around 320 cm^{-1} and 650 cm^{-1} arise from the flexural vibrational modes of graphene. Thus, for heat transfer through graphene the contribution of the flexural phonons perpendicular to the plane of the nanoribbon is significant in comparison to the localized high energy modes along the plane of the 2D nanostructure.

The phonon modes of the nanoribbon are influenced by the isotope substitution that induces a mass disorder to the network of carbon atoms in graphene. We also see from Fig. 5 that with increasing ^{14}C substitution, both the in-plane and out-of-plane vibrational modes shift to lower wavenumbers.[12] The shift, as observed for the peaks in the DOS spectra, is relatively more pronounced for the high energy ones along the in-plane direction than for the flexural modes that have lower wavenumbers. The high energy DOS maximum for ^{12}C (0% substituted) graphene observed at 1350 cm^{-1} shifts to 1200 cm^{-1} for a 100% substituted nanoribbon. The height of the peak corresponding to this mode decreases (with increasing ^{14}C content) from that for the pure ^{12}C nanoribbon until it reaches a minimum for a graphene containing 50% ^{14}C atoms, and then increases again with increasing substitution.

While computing and/or measuring the thermal conductivities of these isotope substituted nanostructures provides a quantitative estimate of how mass disorder influences heat transfer through them, the unanswered question is *which modes of the vibrational spectra are predominantly affected by isotope substitution*;[23,24] *is it the short-ranged high frequency modes or the delocalized low frequency modes? Are the in-plane vibrations or the out-of-plane flexural modes*[25] *that influence thermal transport*? Identifying and correlating the effects of isotopes on the vibrational spectra to the material transport property will provide recommendations to design materials with targeted properties.

We have shown in prior studies the power of using eigenvalue decomposition methods on DOS spectra as means of linking electronic / crystal structure-property relationships[26–30] and in this study we expand this from bulk 3D systems to 2D systems. Specifically, principal component analysis (PCA) is used to extract and identify patterns within the DOS spectra, which identify the correlation between carbon isotope fractions, lattice vibrations and thermal conductivity. The informatics analysis extracts information from the spectra which is otherwise not identified. The DOS profile is decomposed as 10^4 discrete points for nine curves and a total of 10^5 data values are input into the analysis, with each wavenumber considered a unique descriptor or response and each carbon fraction as a separate sample or condition. The values of the response are then the DOS value at each wavenumber. The eigenvalue decomposition then decomposes the DOS spectra into (i) the primary spectral patterns which comprise the DOS and ranked by importance of the patterns in defining changes in DOS with isotope substitution, and (ii) the weighting on each pattern to reconstruct the original DOS. A predictive model between the weights and the thermal conductivity is developed, with the model very efficient due to decomposing the DOS into a

small parameter matrix. The output then is a prediction of thermal conductivity values, which we compare with other calculation approaches here, and a measurement of the impacts on the different phonon modes on the thermal conductivity. Therefore, using PCA, the "hidden" patterns within the DOS spectra and the correlation between carbon isotope fractions, lattice vibrations and thermal conductivity can be mathematically defined.

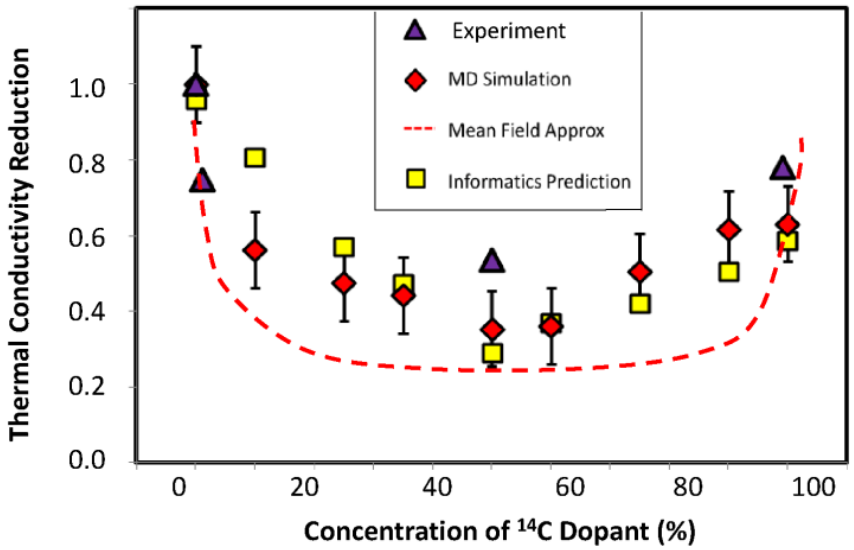

Figure 6. Relationship between informatics analysis of phonon DOS and thermal conductivity. There is good agreement between informatics predictions and MD simulation and both capture the same minima in conductivity with 50% isotope concentration. The predictions also capture the same trends as previous computational[12] and experimental results[35] with differences existing due to different atomic masses of the carbon isotopes. Using informatics, we are able to predict the thermal conductivity of isotope substituted graphene of all possible binary compositions without requiring additional MD calculations or measurements.

The result of the principal component analysis and subsequent high-dimensional regression is shown in Fig. 6. The model is developed to minimize both the root mean square error of the test and training data.[31,32] This result is in good agreement with independently derived computational and experimental results. Given this agreement, we are then able to define the role of localized versus delocalized phonon modes on the thermal conductivity.

Interrogating the eigenvalue spectrum (Fig. 7) allows us to identify through an unsupervised process which aspects of the phonon correspond to features of the original DOS spectrum. The key features of the DOS spectra, including shape of the peaks between 1200 and 2000 cm^{-1}, are identified via the loadings spectra and using well established methods, one can extract correlations between the phonon DOS and transport properties. These features in the eigenvalue spectrum are used as inputs into a principal component regression model to establish predictive formulation for thermal conductivity (Equation 1).

$$\text{Thermal conductivity} = -64.10 \times PC1 + 374.28 \times PC2 + 0.55 \quad (1)$$

While delocalized phonon modes provide the primary contribution to remarkable thermal conductivity in graphene,[22,33,34] our finding of the significance of features greater than 1200 cm^{-1} establishes that the high frequency short ranged vibrations exert a significant influence in reducing heat transfer through the isotope substituted nanomaterials. The features within the DOS spectra which mostly impact the thermal conductivity are identified from the loading spectra. The features in the PC2 loadings spectra are most critical for thermal conductivity, given the much larger coefficient for PC2 in Equation (1). The regions circled in Fig. 7(c) control the thermal conductivity, as the intensity of the loadings values represents the importance of the feature onto the principal component and additionally for the heat transfer. These frequencies are all between 1200 and 1800 cm^{-1} and the thermal conductivity

is thus defined by the localized modes. Specifically, the increase in the intensity of DOS at 1250 cm^{-1} and 1600 cm^{-1} and decrease in DOS at 1450 cm^{-1} best correlate with increasing thermal conductivity.

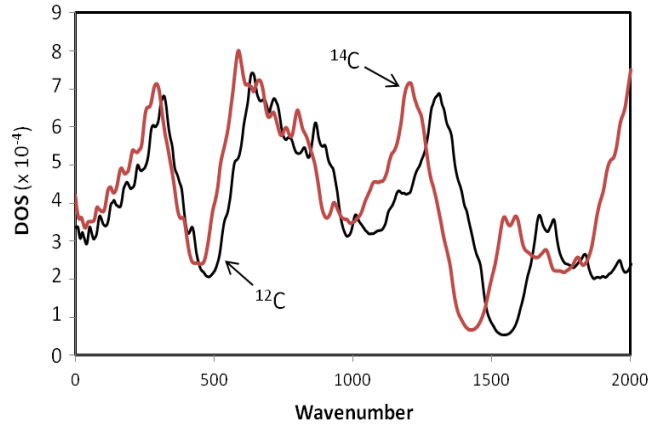

(a)

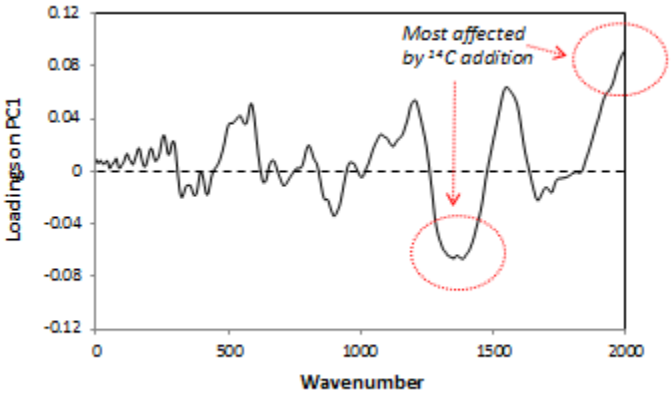

(b)

Figure 7 continued

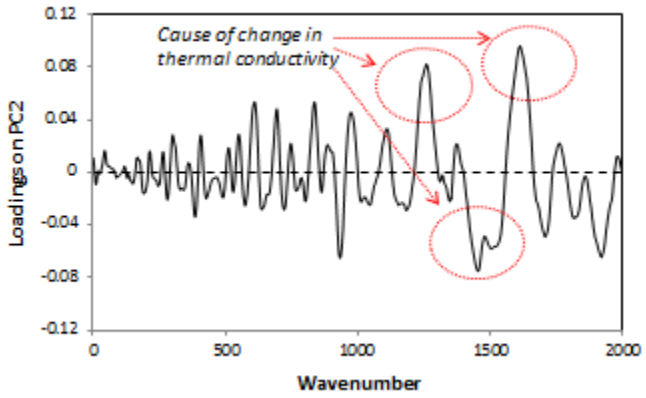

(c)

Figure 7. The modes of the vibrational spectra most affected by changing isotope percentages and resulting in thermal conductivity variation. (a) In isotope substituted materials, high frequency modes are strongly influenced to induce a reduction in thermal conductivity. The loadings spectra capturing relationship between the DOS and isotope concentration is shown in (b), while we also extract the features related to thermal conductivity in (c). The most critical frequencies for thermal conductivity (circled) all are greater than 1200 cm^{-1}, and therefore correspond to localized modes, which are defined as those with wavenumber greater than 800 cm^{-1}. Without employing informatics, we could not have otherwise picked up on the relationship between localized modes and thermal conductivity.

The results obtained from PCA can be understood in light of the fact that heat transfer through graphene is due to the coupled effect of low frequency delocalized modes, which are observed mostly in the out-of-plane direction, and the short ranged high frequency stretching modes along the plane of the material. Presence of mass impurity in the form of heavier isotope perturbs the localized stretching modes due to enhanced phonon scattering, causing a

significant shift in the wavenumbers of the high frequency region to lower values. This in turn induces resultant impedance on the long ranged flexural vibrations, whose wavenumbers show a moderate shift to lower values. In effect, the overall energy transfer by phonons is strongly hindered, as reflected by the drastically reduced thermal conductivities for isotope substituted GNRs.

With this understanding, the selection of materials and incorporation of defects for targeted performance can be streamlined. Further, as shown in Fig. 6, the prediction of thermal conductivity values for isotope substituted graphene is accelerated without requiring additional computationally expensive calculations. For example, we compare our values with previously available thermal conductivity values for mass disordered graphene nanoribbons containing various fractions of ^{14}C isotopes. While earlier experiments[35] show ~ 35% decrease in thermal conductivity when a pure GNR is isotope substituted with 50% of ^{13}C atoms, our results reveal a decrease of ~ 32%. Previous theoretical investigation[36–38] that explain the isotope scattering in GNRs suggest ~ 33% decrease in thermal conductivity for 1% ^{14}C isotope substituted GNRs. Here, in addition to validating these predictions using MD simulations, we propose simple DOS information-driven interpolation techniques to rapidly determine thermal conductivities of mass disordered GNRs containing any fraction of isotopes without actually implementing computationally intensive molecular calculations. Use of the informatics approach enables an acceleration of property calculation and constructs a platform to screen potential material chemistries to discover those with targeted properties. The agreement of the informatics predictions with results from MD simulations (derived following a similar procedure as described elsewhere[12]) and experimental measurements[35] validates the suitability of the data driven approach. We show in this letter

that random isotope substitution in a graphene nanoribbon affects the high frequency modes to reduce the thermal conductivity of the nanomaterials. We conjecture that if the delocalized low frequency modes responsible for the higher thermal conductivities of these nanostructures can be perturbed, even stronger impedance to heat transfer would be possible enabling new material designs with drastically low thermal conductivity values. Thus, our data driven method integrating results of atomistic simulations rapidly has significant implications for providing scaled up transport property predictions. Given a targeted value of material property, say thermal conductivity, our informatics tool can be employed to recommend optimal concentration of ^{14}C isotopes in a graphene structure for hypothesis-driven materials discovery.

We have developed an informatics-based methodology for calculating thermal conductivity as a function of phonon density of states of isotope substituted graphene. Our study has confirmed that localized modes are significant in controlling thermal conductivity. This approach accelerates the prediction of thermal conductivities and reduces the number of atomistic calculations required for graphene nanostructures. Additionally, the informatics tool uncovers the phonon modes that significantly influence thermal transport through these mass disordered graphene nanoribbons. The method and the results derived are validated against predictions from simulations and measurements from previous experiments. Our data driven methodology explores the material fundamentals associated with variations in lattice vibrations of graphene containing isotope impurities and simultaneously accelerates the discovery of nanomaterial chemistries with desired properties, as demonstrated through our predictions of thermal conductivity values.

Acknowledgements: The research reported in this paper is partially supported by the HPC equipment, CyEnce, purchased through NSF MRI grant number CNS 1229081 and NSF CRI grant number 1205413. SB, SS and KR acknowledge support from Air Force Office of Scientific Research (AFOSR) grant number FA9550-12-0496, NSF-ARI Program CMMI 09-3890182 and NSF grant numbers DMS-11-25909 and DMR-13-07811. KR also acknowledges support from the Wilkinson Professorship of Interdisciplinary Engineering.

References

1. K. Ziegler, Phys. Rev. Lett. **97**, 266802 (2006).

2. S. Stankovich, D.A. Dikin, G.H.B. Dommett, K.M. Kohlhaas, E.J. Zimney, E.A. Stach, R. D. Piner, S. T. Nguyen and R.S. Ruoff, Nature **442**, 282 (2006).

3. A.A. Balandin and D.L. Nika, Mater. Today **12**, 266 (2012).

4. K.M.F. Shahil and A.A. Balandin, Solid State Commun. **152**, 1331 (2012).

5. K.S. Novoselov, V.I. Fal'ko, L. Colombo, P. R. Gellert, M. G. Schwab and K. Kim, Nature **490**, 192 (2012).

6. E. Pop, V. Varshney and A.K. Roy, MRS Bull. **37**, 1273 (2012).

7. A. Balandin, S. Ghosh, W. Bao, I. Calizo, D. Teweldebrhan, F. Miao and C.N. Lau, Nano Lett. **8**, 902 (2008).

8. S. Ghosh, I. Calizo, D. Teweldebrhan, E.P. Pokatilov, D.L. Nika, A.A. Balandin, W. Bao, F. Miao and C. N. Lau, Appl. Phys. Lett. **92**, 151911 (2008).

9. J.H. Seol, I. Jo, A.L. Moore, L. Lindsay, Z.H. Aitken, M.T. Pettes, X. Li, Z. Yao, R. Huang, D. Broido, N. Mingo, R.S. Ruoff and L. Shi, Science (80). **328**, 213 (2010).

10. C. Sevik and G. Cuniberti, Nano Lett. **11**, 4971 (2011).

11. U. Ray and G. Balasubramanian, Chem. Phys. Lett.**599**, 154–158, (2014).

12. G. Balasubramanian, I. K. Puri, M. C. Böhm and F. Leroy, Nanoscale **3**, 3714 (2011).

13. J.R. Lukes and H.Zhong, J. Heat Transfer **129**, 705 (2007).

14. J. Martin, N. Akerman, G. Ulbricht, T. Lohmann, J.H. Smet, K. Von Klitzing and A. Yacoby, Nat. Phys. **4**, 144 (2007).

15. S. Plimpton, J. Comput. Phys. **117**, 1 (1995).

16. J. Tersoff, Phys. Rev. B **39**, 5566 (1989).

17. L. Lindsay and D.A. Broido, Phys. Rev. B **81**, 205441 (2010).

18. W. Humphrey, A. Dalke and K. Schulten, J. Mol. Graph. **14**, 33 (1996).

19. F. Leroy, J. Schulte, G. Balasubramanian and M.C. Böhm, J. Chem. Phys. **140**, 144704 (2014).

20. M. Alaghemandi, F. Müller-Plathe and M.C. Böhm, J. Chem. Phys. **135**, 184905 (2011).

21. M. Alaghemandi, F. Leroy, F. Müller-Plathe and M.C. Böhm, Phys. Rev. B **81**, 125410 (2010).

22. D. Donadio and G. Galli, Phys. Rev. Lett. **102**, 195901 (2009).

23. J. Turney, E. Landry, A. McGaughey and C. Amon, Phys. Rev. B **79**, 064301 (2009).

24. D. Donadio and G. Galli, Phys. Rev. Lett. **99**, 255502 (2007).

25. D. L. Nika, E. P. Pokatilov and A.A. Balandin, Phys. Status Solidi (B). **248**, 2609 (2011).

26. S.R. Broderick and K. Rajan, Europhys. Lett. **95**, 57005 (2011).

27. S. R. Broderick, H. Aourag and K. Rajan, J. Am. Ceram. Soc. **94**, 2974 (2011).

28. S.R. Broderick, C. Suh, J. Provine, C.S. Roper, R. Maboudian, R. T. Howe and K. Rajan, Surf. Interface Anal. **44**, 365 (2012).

29. S.R.Broderick, H. Aourag, and K. Rajan, Stat. Anal. Data Min. **6**, 353 (2009).

30. S.R.Broderick, J. R. Nowers, B. Narasimhan and K. Rajan., J. Comb. Chem. **12**, 270 (2010).

31. S. Chatterjee and B. Price, Biometrical J. **34**, 734 (1991).

32. A.N. Andriotis, G. Mpourmpakis, S. Broderick, K. Rajan, S. Datta, M. Sunkara and M. Menon, J. Chem. Phys. **140**, 094705 (2014).

33. L. Lindsay, D. A. Broido and N. Mingo, Phys. Rev. B **80**, 125407 (2009).

34. L. Lindsay, D. A. Broido and N. Mingo, Phys. Rev. B **83**, 235428 (2011).

35. S. Chen, Q. Wu, C. Mishra, J. Kang, H. Zhang, K. Cho, W. Cai, A. A. Balandin and R.S. Ruoff, Nat. Mater. **11**, 203 (2012).

36. Z. Johari, M.T. Ahmadi, D. C. Y. Chek, N. A. Amin and R. Ismail, J. Nanomater. **2010**, 1 (2010).

37. D. Nika, E. Pokatilov, A. Askerov and A. A. Balandin, Phys. Rev. B **79**, 155413 (2009).

38. V. Adamyan and V. Zavalniuk, J. Phys. Condens. Matter **24**, 415401 (2012).

CHAPTER 4. DISSIMILAR HEAT CONDUCTION MECHANISMS IN ANALOGOUS 2D NANOMATERIALS WITH ISOTOPE SUBSTITUTION: GRAPHENE VERSUS SILICENE

Modified from a paper to be submitted for archival publication

Upamanyu Ray[1] and Ganesh Balasubramanian[2]

Abstract

It is shown that although graphene and silicene are structurally similar two-dimensional analogous nanomaterials, they have drastically different heat conduction mechanisms. Employing molecular dynamics simulations, we examine the phonon spectra of these nanomaterials and reveal that the out-of-plane flexural modes that exert a dominant contribution towards heat transfer in graphene, are essentially nonexistent for silicene. In contrast, heat conduction in silicene is predominantly due to in-plane acoustic vibrations transverse to the direction of heat transfer. These differences arise from the relatively weaker bond strength in silicene causing reduced phonon group velocity, but more importantly due to the buckling of the silicon nanomaterial that does not have an exact planar conformation as graphene. Coupling of the out-of-plane and longitudinal modes causes mode softening in the direction of thermal transport. Despite the differences in the dominant phonon modes, both silicene and graphene exhibit similar variations in thermal conductivity with increasing isotope substitution. Heat transfer in mass disordered nanomaterials is reduced because of the shift in characteristic phonon frequencies to lower values indicating reduced energy carrying capacity, and through energy scattering by phonons at the isotope sites. Predictions of the

[2]Corresponding author
Department of Mechanical Engineering,
2092 Black Engineering,
Iowa State University, Ames, IA 50011, USA
Tel.: +1 -515-294-9226
Email: bganesh@iastate.edu

thermal conductivity reduction, which is stronger in graphene than in silicene, agree with results of an analytical model based on mean-field approximation.

Thermal transport in graphene, a planar sheet of sp^2-bonded carbon atoms in a honeycomb lattice, has been extensively investigated over the last decade using both experimental[1,2] and theoretical[3] approaches. While the high thermal conductivities of graphene are attractive for thermal management applications, its ability to conduct charges could potentially revolutionize the electronic industry.[4] In particular, defect engineered graphene nanostructures with reduced thermal conductivities are potential candidates for high frequency applications and circuits that require low flicker noise.[5–9] Analogous to the planar graphene, a stable hexagonal arrangement of silicon atoms in a two-dimensional (2D) structure with some local buckling, termed as silicene, has been gaining attention recently,[8,10] due to its high crystallinity, unique electrical transport properties such as tunable band gaps[11,12] as well as low thermal conductivity[13,14] that make it an attractive nanomaterial for refrigeration and power generation applications.[15,16] Given the billions of dollars invested in establishing the silicon industry, if silicene can be enabled to produce remarkable transport properties similar to graphene for electronic and thermoelectric applications, one can envision a transformative progress in the area of semiconductor devices.[17,18]

Energy transport in both these 2D materials is known to occur predominantly by lattice vibrations (or phonons). Silicene, although similar in geometry to the graphene, contains ordered structural undulations that can contribute to differences in the phonon modes characteristic to heat transfer than what has been observed for graphene. The few fundamental investigations available in the literature[13,14,19] offer inconsistent predictions, emphasizing the need for an accurate understanding of the underlying mechanisms driving the heat transport in silicene as compared to graphene. The complexity is further increased if there is mass disorder in these materials due to presence of defects of different forms, such as isotopes, vacancies, dopants etc., and correlating the thermal conductivity variation with the changes in the phonon spectra is nontrivial and necessary to thoroughly describe the thermal transport characteristics of silicene.

Presence of isotopes in a material structure induces mass disorder, reducing phonon thermal conductivity (*k)* due to enhanced energy scattering for even the slightest defect concentration,

without influencing the electronic properties. The reductions in thermal conductivity for isotope substituted carbon and silicon nanomaterials has been discussed in the literature.[20–25] Nevertheless, there are ambiguities in identifying the dominant vibrational modes contributing to the thermal conductivity of silicene. Two major schools of thought include those who believe that, similar to graphene, heat transfer through silicene is mostly dominated by out-of-plane flexural modes,[13] while an alternative theory[19] proposes that the out-of-plane vibrational modes contribute negligibly to the thermal transport in silicene and heat conduction occurs predominantly due to in-plane modes transverse to direction of energy transfer. Here, we employ molecular dynamics (MD) simulations to understanding the physics of heat transfer in silicene, relative to graphene, by examining the role of different vibrational modes in both the pure and isotope substituted nanomaterials. Of the many isotopes of carbon and silicon, we substitute the ^{12}C and ^{28}Si atoms in the corresponding 2D structures with ^{14}C and ^{30}Si respectively. While ^{14}C is the longest living and heaviest of all the naturally occurring carbon isotopes, ^{30}Si is a very stable atom of silicon. Also, for the sake of consistency, we maintain a difference of 2 units in the atomic masses of the pure atom and its isotope in both the carbon and silicon nanomaterials. Our results, as elaborated below, show major differences in the contributions of the in-plane and out-of-plane phonon modes in structurally analogous graphene and silicene, while the predicted thermal conductivity reductions exhibit a similar trend that is suitably represented by a mean-field approximation model.

Results and Discussion

Graphene and silicene nanoribbons (GNR and SNR, respectively) of length 140 nm (*x*-direction) and width 4.32 nm (*y*- direction) are employed in our MD simulations as shown respectively in Figures 8a and 9a. Upon equilibration of the nanomaterial at 300 K and 0.1 MPa pressure, we find that the relaxed structure of GNR along the *x*-*z* plane shows no buckling or undulations and attains a perfect 2D planar shape (shown in Figure 8b). Thermal transport in 2D nanomaterials is due to the three acoustic phonon modes: in-plane longitudinal mode along *x*-direction, in-plane transverse mode along *y*-direction and out-of-plane flexural mode in the *z*- direction. Low frequency long-range modes contribute the most towards conduction of energy, while high frequency localized vibrations represent short

ranged stretching modes whose role in thermal transport is limited. Isotope substitution contributes to mass disorder, that in turn results in perturbation of the vibrational modes. Hence, to understand the role of isotopes in thermal transport, a comprehensive knowledge of the changes in the phonon spectra, or the vibrational Density of States (DOS), with isotope concentration is required. We examine the characteristics of the three vibrational modes by computing the phonon DOS for isotope substitution percentages of 0%, 10%, 25%, 30%, 35%, 50%, 60%, 75%, 90% and 100%. For the sake of clarity we show only the DOS curves for 0%, 50% and 100% isotope substitution in Figure 8, as they represent the extreme cases. The DOS curves for GNR along the *x*-, *y*- and *z*- directions are presented Figure 8c, 8d and 8e respectively. Along both the longitudinal (*x*) and transverse (*y*) in-plane directions, the phonon spectra presented in Figures 8c and 8d shows that the majority of the vibrational modes are high energy localized ones with peaks at around 66 Terahertz (THz) and 37 THz, in agreement with earlier literature.[25] The vibrations along the plane of the GNR are short-range stretching modes that scatter energies and have a relatively lower contribution to heat transfer. On the other hand, the DOS spectra perpendicular to the direction of heat transfer in the out-plane direction[25,26] peaks at much lower phonon frequencies of 9 THz and 20 THz as shown in Figure 8e. These flexural modes have lower energies but are delocalized and hence propagate farther than the in-plane vibrations along the *x*- and *y*-directions. Thus, although the structure of the GNR is planar, the dominant contributions to heat transfer and the remarkably high thermal conductivities are attributed to the out-of-plane long-range phonons. The effect of mass disorder is also very conspicuous for the vibrational modes in all three directions. With increasing isotope fraction from 0% to 100%, the frequencies of the vibrational modes shift to lower values[27] as shown in Figures 8c, 8d and 8e. The shifts, explicitly identifiable for the peak frequencies, are more prominent in the higher frequency range for the short-ranged phonons than for low frequency delocalized vibrational modes. Lowered frequencies indicate reduced energy carrying capacity of the phonon modes. With increasing isotope concentration, more fractions of heavier masses are incorporated into the 2D structure. The heavier the mass, the greater the energy required for its vibration, and lower is its capacity to transfer the vibrational energy throughout the nanomaterial. The shift of the DOS spectra to lower frequencies illustrates the effect of mass disorder on the vibrational characteristics of GNR.

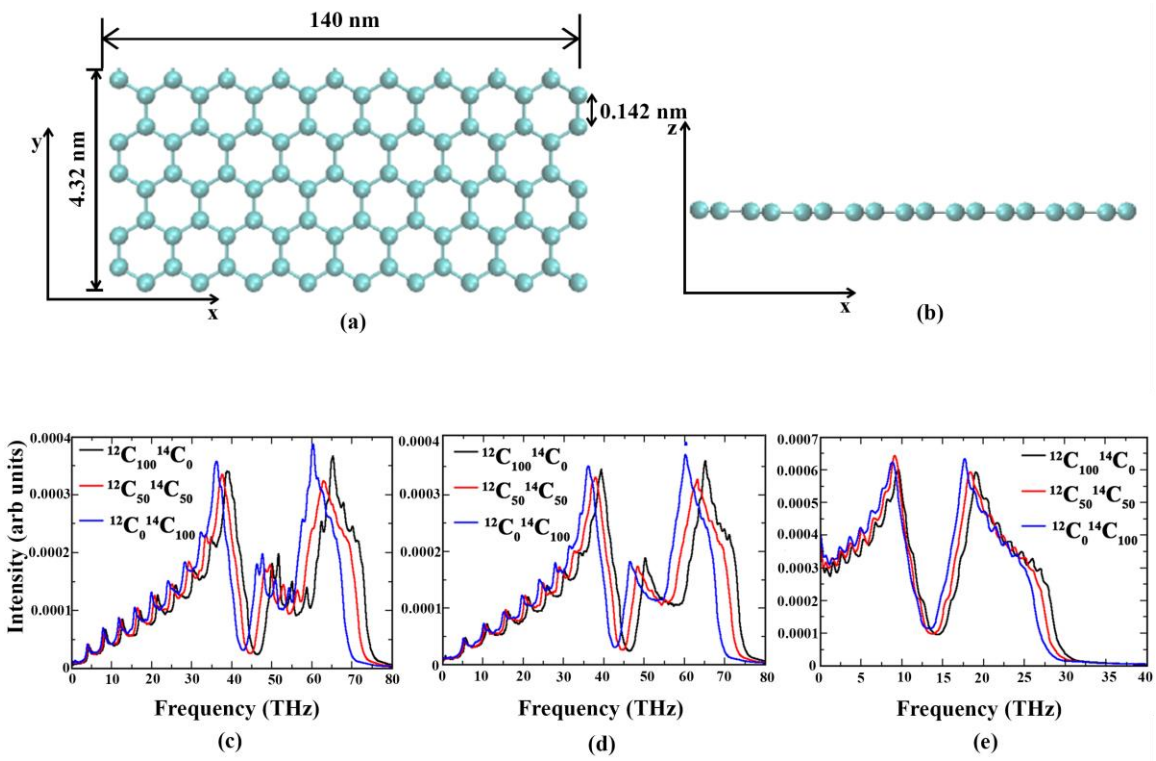

Figure 8. The equilibrated structure of GNR of length *L*= 140 nm and width= 4.32 nm along the *x*-*y* snd *x*-*z* planes is shown in (a) and (b) respectively. C-C bond length in GNR is 0.142 nm. The view of the nanomaterial along the *x*-*z* plane shows that GNR has no buckling in the structure and has an exact planar conformation. The phonon DOS for 0% (black), 50% (red) and 100% (blue) isotope substituted GNR are presented for the (c) in-plane longitudinal modes along the direction (*x*-wise) of heat transfer, (d) in-plane transverse modes (*y*-wise) and (e) out-of-plane flexural modes perpendicular (*z*-wise) to the direction of heat transfer. The DOS intensity represented along the vertical axes of (c), (d) and (e) is in arbitrary units. The legends represent each GNR structure as $^{12}C_{(100-100\phi)}{}^{14}C_{100\phi}$,, where ϕ is the ^{14}C isotope substitution fraction. Along *x*-direction, the phonon frequency peaks occur around 66 THz and 37 THz for pure (black) GNR ($^{12}C_{100}{}^{14}C_0$), around 62.5 THz and 36 THz for 50% (red) isotope substituted GNR ($^{12}C_{50}{}^{14}C_{50}$) and around 60 THz and 34 THz for 100% isotope substituted (blue) GNR ($^{12}C_0{}^{14}C_{100}$). The phonon frequencies shift to lower values for the in-plane vibrational modes along both the *x*- and *y*- directions. Along *z*-direction,

the phonon spectra shift occurs from around 20 THz and 9 THz for pure GNR to around 17.5 THz and 8 THz for 100% isotope substituted cases. The low frequency delocalized modes observed along the *z*-direction exert significant contributions towards heat transfer in GNR.

A similar analysis is performed for SNR to understand if any differences exist in its heat conduction mechanisms relative to that of the analogous carbon nanomaterial. Upon equilibration of the SNR (shown in Figure 9a) of similar dimensions as the GNR, an exact planar conformation of the 2D material is not observed. Instead, unlike graphene, there is an ordered undulation in the lattice structure that results in an effective buckling height (*h*) of 0.067 nm along the *x*-*z* plane, as shown in Figure 9b. The geometry of our equilibrated structure agrees very well with earlier investigations of silicene, that report an *h* value between 0.020 nm to 0.100 nm.[10,14,19,28] The differences arise due to different equilibration procedures, which includes use of different intermolecular potential functions for describing the atomic interactions in silicene. Our choice of Tersoff potential is able to correctly replicate the buckling effect, and hence is a suitable choice to understand thermal transport characteristics of silicene. Although graphene and silicene are analogous 2D materials,[29,30] their structural configurations are not exactly similar with SNR deviating from the perfect planar lattice form.

The phonon DOS for SNR along the *x*-, *y*- and *z*- directions are shown in Figures 9c, 9d and 9e. The vibrational spectra along the in-plane directions for pure SNR shows peak intensities at frequencies of 17.5 THz and 7 THz for both the transverse i.e. *y*-wise (Figure 9d) as well as longitudinal i.e. *x*-wise modes (Figure 9c). The frequency range for both these being much lower than that of GNR, we conjecture that these modes depict the long-range phonons that are delocalized and transport energy along the *x*-*y* plane of the SNR. A closer examination reveals that the transverse modes have a greater abundance of these low frequency vibrations than those along the direction of heat transfer where we find an effect of mode softening due to coupling with the out-of-plane modes, discussed later. In the out-of-plane direction, we do

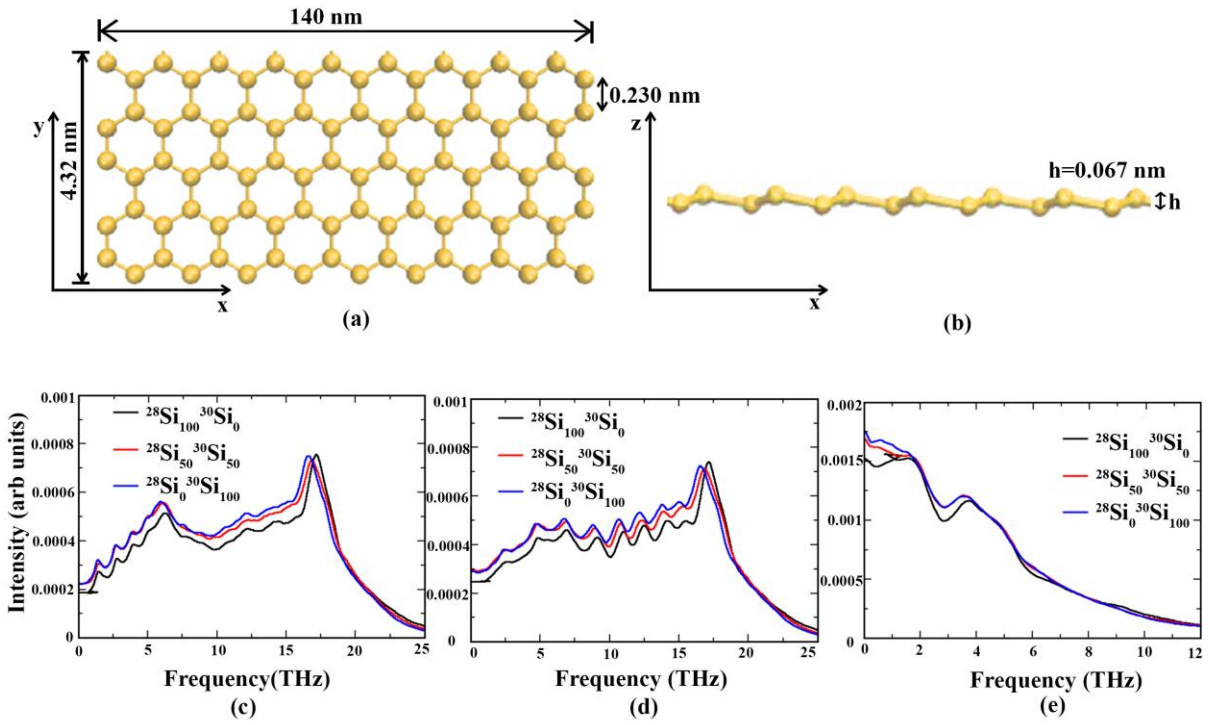

Figure 9. The equilibrated structure of SNR of length *L*= 140 nm and width= 4.32 nm along the *x*-*y* snd *x*-*z* planes is shown in (a) and (b) respectively. Si-Si bond length in SNR is 0.230 nm. The view of the nanomaterial along the *x*-*z* plane shows that SNR has regular undulations and is not exactly planar. An effective buckling height is computed to be 0.067 nm. The phonon DOS for 0% (black), 50% (red) and 100% (blue) isotope substituted SNR are presented for the (c) in-plane longitudinal modes along the direction (*x*-wise) of heat transfer, (d) in-plane transverse modes (*y*-wise) and (e) out-of-plane modes perpendicular (*z*-wise) to the direction of heat transfer. The DOS intensity represented along the vertical axes of (c), (d) and (e) is in arbitrary units. The legends represent each GNR structure as $^{28}Si_{(100-100\phi)}$ $^{30}Si_{100\phi}$, where ϕ is the ^{30}Si isotope substitution fraction. Along *x*-direction, the phonon frequency peaks that occur around 17.5 THz and 7 THz for pure (black) SNR ($^{28}Si_{100}$ $^{30}Si_0$), shift to 16.5 THz and 6 THz for 50% (red) isotope substituted SNR ($^{28}Si_{50}$ $^{30}Si_{50}$) and to 16 THz and 5.5 THz for 100% isotope substituted (blue) SNR ($^{28}Si_0$ $^{30}Si_{100}$). The in-plane transverse vibrational modes along the *y*-direction also exhibit a frequency shift from around 17.5 THz in $^{28}Si_{100}$ $^{30}Si_0$, to 17 THz in $^{28}Si_{50}$ $^{30}Si_{50}$ and finally to 16 THz in $^{28}Si_0$ $^{30}Si_{100}$. There is a mode softening effect in the direction of heat transfer, and a strong population of delocalized phonon

modes along the *y*- axis, transverse to the heat conduction direction. Along *z*-direction, the phonon spectra does not produce any noticeable vibrational modes apart from that around 3.9 THz for pure SNR which shifts to around 3.6 THz for 100% isotope substitution. The buckling effect in SNR restricts the contributions of out-of-plane acoustic vibrations to heat conduction to almost zero, which is contrary to the mechanism observer for GNR. In silicene, the in-plane transverse modes exert significant contributions towards heat transfer.

not find notable DOS spectra, with only minor vibrational modes observed around 3.9 THz. This implies that out-of-plane phonons exert negligible contribution to thermal conductivity of silicene. Furthermore, the lack of identifiable out-of-plane modes suggests an absence of flexural vibrations along the *z*-axis. Instead, the buckling of the SNR lattice results in weak acoustic modes normal to the plane of the nanomaterial while the other components of the vibrations are coupled to the in-plane longitudinal modes creating a mode softening effect. Additionally, it is important to note that the Si-Si bond strength in silicene is relatively weaker to that of C-C in graphene. This reduces the group velocity of the out-of-plane phonons in SNR, limiting the contributions of these modes to thermal transport to almost zero. Thus, in spite of being a material analogous to graphene, heat conduction in SNR is predominantly due to in-plane phonons transverse to the direction of heat transfer while for GNR it is the out-of-plane flexural modes. This is a fundamental difference in the heat conduction mechanism of two comparable 2D materials both having a similar honeycomb lattice structure.

The influence of mass disorder in shifting the vibrational spectra towards lower frequencies in SNR follows similar trend as in GNR. Figures 9c and 9d explicitly reveal that 0%, 50% and 100% isotope substitution in silicene lower the characteristic frequencies of the phonon modes along the *x*-*y* plane. Again, as before, a lower frequency implies a reduced energy carrying capacity and is detrimental to heat transfer by acoustic in-plane vibrations. The shift is prominent for the peak frequencies. For the out-of-plane direction, phonon modes are sparse and hence no noticeable shifts can be demonstrated in the frequencies. While the underlying mechanisms and dominant phonon modes governing heat conduction in graphene and silicene are markedly different, the effect of mass disorder causing the transition of

acoustic vibrations towards lower frequencies and subsequently reducing the energy carrying capacity of the phonons, is similar for both the 2D nanomaterials.

Next, we examine whether the difference in heat conduction mechanisms in SNR and GNR are reflected in their respective thermal conductivity (k) reductions with increasing isotope concentration. We show in Figure 10 that with increase in isotope fraction (ϕ), k initially decreases till the isotope concentration is 50%. Beyond ϕ=0.5, k again increases representing the characteristic U-shaped curve.[27,31] Increasing the fraction of isotopes from 0 till 0.5 induces a gradual increase in mass disorder. Atoms in the nanoribbon lattice are either the lighter ^{12}C (for GNR) and ^{28}Si (for SNR) or correspondingly the heavier ^{14}C and ^{30}Si. The vibrational frequencies of the 2D nanomaterial shift to lower values with increasing isotope fraction as discussed in Figures 8 and 9, reducing the energy carrying capacity and hence the thermal conductivity. Additionally, the characteristic vibrational frequencies of the heavier and lighter masses are different. When both of the isotopes are present in a lattice, scattering of energies carried by phonons of different frequencies occurs. k decreases till it reaches a minimum at 50% isotope substitution as the mass disorder causes localization of phonon modes and lowers the phonon group velocity. While frequencies continue to shift to lower values with further increase of isotope concentration, in contrast k increases for $0.5 < \phi < 1.0$. For isotope concentration between 50% and 100% the heavier atoms comprise the majority of the 2D lattice structure. As mass disorder decreases, energy losses due to phonon scattering is reduced and heat conduction is improved, as reflected in the increasing values of k. Also, it is important to note that inclusion of a low fraction of mass disorder induces a relatively significant reduction in k,[32,33] whereas the variations in thermal conductivity are relatively less for further increase in isotope concentration. This drastic decrease in k for low isotope percentage is more prominent in GNR than in SNR. For nanomaterials of the same dimensions, the phonon mean free path in SNR is around $1.35L$,[28] where L is the length of the nanoribbon. Here, this is 189 nm. The corresponding value for GNR is much longer, and for our simulations it is 775 nm.[34] For similarly sized materials, a longer mean free path leads to increased phonon scattering at the isotope sites and at the material boundaries, increases resistance to thermal transport through the material and impedes heat conduction. Subsequently, we observe a stronger reduction in k for graphene even though the trend of relative decrease in thermal conductivity is similar for both GNR and SNR. We predict a

maximum k reduction of about 71.6% in 50% isotope substituted GNR and 21.7% for the corresponding SNR with respect to the k values of the respective isotopically pure structures. We compare our k reduction predictions with a classical model based on mean-field approximation[27] that proposes the heat transfer reduction [$k(\phi)$] as:

$$k(\phi)=k_\phi/k_0 = \sqrt{\frac{\varepsilon(1+\varepsilon)[(1-\phi+\varepsilon)M_\alpha+(\phi+\varepsilon)M_\beta]}{(\phi+\varepsilon)(1-\phi+\varepsilon)[(1+\varepsilon)M_\alpha+\varepsilon M_\beta]}}, \quad (1)$$

where k_ϕ is the thermal conductivity of isotope substituted nanoribbon, k_0 is the thermal conductivity of the pure nanomaterial, ϕ is the molar fraction of the isotope β that replaces atom α in the nanoribbon, M stands for the effective isotope masses and ε is a dimensionless numerical parameter to prevent divergence for the limiting cases.[27] Applying the constraints of $k(0)=1$, $k(1)=k_{100}/k_0$ and $k(0.5)= k_{50}/k_0$ using the values computed from the MD simulations, we find the values of the parameter ε, M_α and M_β. The values of ε for GNR and SNR are 0.024289 and 0.3633264 respectively and the ratio of M_α/M_β equals 1.30878 for GNR and 0.95185 for SNR. The k reduction model in equation (1) is presented in Figure 10 for both GNR and SNR. The model predictions compare very well with the results calculated from the atomistic simulations. While remarkable qualitative agreement is observed, the minor quantitative differences exist due to the limited sampling data used for computing k values instead of averaging over a series of calculations with different spatial isotope arrangements. The mean-field approximation model reproduces the significant decrease in k for low isotope fraction and the relatively lower reduction when the mass disorder is between 30% and 70% for both the nanoribbons. The predictions of the model, which requires only the masses of the atoms and fraction of isotopes, in combination with the DOS spectra for the mass disordered GNR and SNR, we corroborate that it is the perturbation of the dominant modes of the C and Si atoms in both the nanomaterials that is responsible for the reduction in thermal conductivity. However, it is interesting to note that although the phonon transport mechanisms underlying the heat conduction is different in the analogous 2D materials with isotope substitution, the k reduction with mass disorder follows a similar trend.

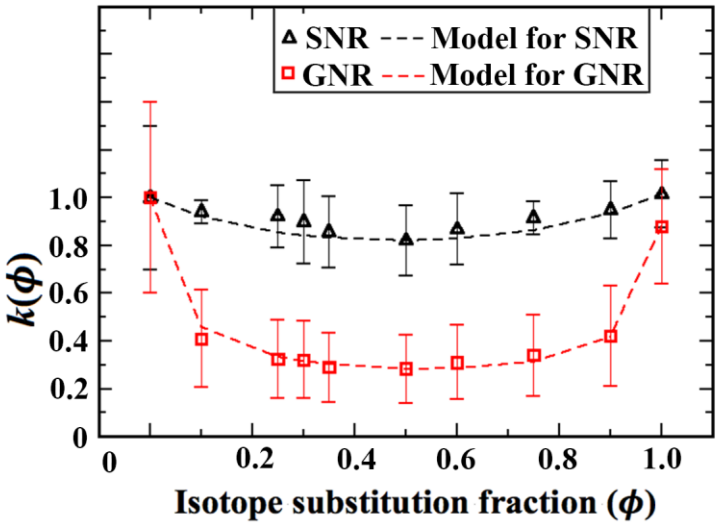

Figure 10. The variation of the thermal conductivity reduction $k(\phi)$ of mass disordered SNR and GNR is presented as the function of increasing isotope substitution fractions (ϕ) from 0.0 –1.0 for nanomaterials simulated at 300 K and 0.1 MPa pressure. The error bars represent the standard errors computed from the different simulations. Thermal conductivity calculations from the MD simulations show reasonable agreement with the predictions of mean-field approximation model given equation (1), shown here as the dashed black curve for SNR and the dashed red curve for GNR. The model reproduces the sharp drop in k due to the presence of smaller isotope fractions as well as the maximum reduction in k due to 50 % isotope substitution in both the nanomaterials. The values of the dimensionless parameter ε used in our calculations are 0.3633264 for SNR and 0.024289 for GNR. For GNR, the value of M_α/M_β = 1.30878 and for SNR, the value of M_α/M_β = 0.95185.

Conclusions

In summary, our computational investigation employing molecular simulations reveals that two nanomaterials, graphene and silicene, with analogous 2D honeycomb lattice structures have dissimilar dominant vibrational characteristics contributing to the heat conduction mechanism. Heat conduction in SNR is predominantly due to in-plane phonons transverse to the direction of heat transfer, while for GNR it is the out-of-plane flexural modes. Such a fundamental difference in thermal transport mechanism is attributed to (1) the buckled

structure of SNR in comparison to the planar conformation of GNR, and (2) the lower phonon group velocities in silicene because of the weaker Si-Si bond strength relative to that between carbon atoms in graphene. Regardless of this difference, in presence of isotopes that induces a mass disorder in the material structure, thermal conductivity reductions in these nanomaterials is ascribed essentially to the perturbation of the dominant phonon modes. Vibrational frequencies illustrated via the DOS spectra shift to lower values demonstrating a reduced energy carrying capacity of the phonons. Additionally, phonons arising from atoms with dissimilar masses lead to energy scattering at the impurity sites, which further contributes in reducing *k* of isotope substituted 2D materials. Stronger reductions are observed for GNR than in SNR. This is due to the relative longer mean free path of phonons in graphene that enhances resistance to heat transfer especially at material boundaries and isotope sites. Qualitatively, the variations of *k* with increasing isotope substitution percentages are similar in both GNR and SNR. A model for thermal conductivity reduction based on mean-field approximation, and, simply considering the masses and fractions of the two isotopes, provides *k* predictions that compare very well with our atomistic simulations. Thus, although the underlying processes contributing to heat conduction in analogous 2D nanoribbons of graphene and silicene) are dissimilar, thermal conductivity variations with mass disorder through isotope substitution in both these nanomaterials are primarily driven by changes in the vibrational characteristics of dominant phonon modes with quantitative differences existing only due to structure specific properties.

Methods

MD simulations are employed to investigate thermal transport in nanoribbons of silicene and graphene. The chirality of both these nanostructures is of the armchair (10,10) form. Each of the nanoribbons extends for 140 nm in *x*-direction and 4.32 nm in *y*-direction, with *x*-being the direction of heat conduction. The Si-Si bond length in silicene is 0.230 nm while the C-C bond in graphene is 0.142 nm long. Due to the difference in bond lengths and diameters of Si and C, the number of atoms in silicene nanoribbon (SNR) and graphene nanoribbon (GNR) are different even though their dimensions are exactly same. Both the nanoribbons are one atom thick with the respective van der Waals diameter being 0.34 nm for C and 0.42 nm for Si atom.[13] We randomly substitute ^{12}C and ^{28}Si atoms in the respective nanoribbons with

their heavier counterparts, ^{14}C isotope in case of GNR and ^{30}Si for SNR. The different isotope substitution percentages we consider in our simulations are 0%, 10%, 25%, 30%, 35%, 50%, 60%, 75%, 90% and 100%.

Periodic boundary conditions (PBCs) are imposed in all directions. The *y*- and *z*- wise dimensions of the simulation box are kept substantially large (*y*-axes: 50 nm and *z*-axes: 200 nm) to prevent the nanoribbons from interacting with their own periodic images along these axes. The widely employed 3-body Tersoff potential is used to model the Si-Si and C-C interactions.[35] The highly parallelized LAMMPS package[36] is used to perform all the simulations in our investigation and VMD tools are used for the visual analyses.[37]

Each structure is initialized at a temperature of 300 K and a pressure of 0.1 MPa and equilibrated using isothermal-isobaric, canonical and microcanonical ensembles as described earlier.[25,27] This is succeeded by computations of the averaged mass-weighted velocity autocorrelation function (VACF) to derive the phonon density of states (DOS) spectra, following the same procedure as detailed elsewhere.[25] The *z*- axis represents the out-of-plane direction and the in-plane axes are along the *x*- and *y*- directions. *k* is computed using the popular reverse non-equilibrium MD (RNEMD) technique.[14] Again, explanation about the implementation of this method is available in our earlier work.[25] It is important to note that for the cross-section area used in the *k* calculation we simply consider a rectangular region with the width (*y*-axis) equal to 4.32 nm and thickness equal to the van der Waals diameter of the C or Si atom for GNR and SNR respectively.[13,25]

Acknowledgement. The work was supported by the National Science Foundation (NSF) grant no. CMMI-1404938. We acknowledge the use of the HPC equipment CyEnce, purchased through NSF MRI grant number CNS 1229081 and NSF CRI grant number 1205413, for the simulations.

References and Notes

(1) Ghosh, S.; Calizo, I.; Teweldebrhan, D.; Pokatilov, E. P.; Nika, D. L.; Balandin, A.; Bao, W.; Miao, F.; Lau, C. Extremely High Thermal Conductivity of Graphene: Prospects for Thermal Management Applications in Nanoelectronic Circuits. *Appl. Phys. Lett.***2008**, *92*, 151911.

(2) Seol, J.; Jo, I.; Moore, A.; Lindsay, L.; Aitken, Z.; Pettes, M.; Li, X.; Yao, Z.; Huang, R.; Broido, D.; *et al.* Two-Dimensional Phonon Transport in Supported Graphene. *Science***2010**, *328*, 213–216.

(3) Zhang, H.; Lee, G.; Fonseca, A. F.; Borders, T. L.; Cho, K. Isotope Effect on the Thermal Conductivity of Graphene. *J. Nanomater.***2010**, *2010*, 1–5.

(4) Pop, E.; Varshney, V.; Roy, A. K. Thermal Properties of Graphene: Fundamentals and Applications. *MRS Bull.***2012**, *37*, 1273–1281.

(5) Yang, X.; Liu, G.; Balandin, A. A.; Mohanram, K. Triple-Mode Single-Transistor Graphene Amplifier and Its Applications. *ACS Nano***2010**, *4*, 5532–5538.

(6) Goli, P.; Ning, H.; Li, X.; Lu, C. Y.; Novoselov, K. S.; Balandin, A. A. Thermal Properties of Graphene-Copper-Graphene Heterogeneous Films. *Nano Lett.***2014**, *14*, 1497–1503.

(7) Shahil, K. M. F.; Balandin, A. A. Graphene-Multilayer Graphene Nanocomposites as Highly Efficient Thermal Interface Materials. *Nano Lett.***2012**, *12*, 861–867.

(8) Yan, Z.; Liu, G.; Khan, J. M.; Balandin, A. A. Graphene Quilts for Thermal Management of High-Power GaN Transistors. *Nat. Commun.***2012**, *3*, 827.

(9) Varshney, V.; Patnaik, S. S.; Roy, A. K.; Froudakis, G.; Farmer, B. L. Modeling of Thermal Transport in Pillared-Graphene Architectures. *ACS Nano***2010**, *4*, 1153–1161.

(10) Vogt, P.; De Padova, P.; Quaresima, C.; Avila, J.; Frantzeskakis, E.; Asensio, M. C.; Resta, A.; Ealet, B.; Le Lay, G. Silicene: Compelling Experimental Evidence for Graphenelike Two-Dimensional Silicon. *Phys. Rev. Lett.***2012**, *108*, 155501.

(11) Tsai, W.; Huang, C.; Chang, T.; Lin, H.; Jeng, H.; Bansil, A. Gated Silicene as a Tunable Source of Nearly 100% Spin-Polarized Electrons. *Nat. Commun.***2013**, *4*, 1500.

(12) Du, Y.; Zhuang, J.; Liu, H.; Xu, X.; Eilers, S.; Wu, K.; Cheng, P.; Zhao, J.; Pi, X.; See, K. W.; *et al.* Tuning the Band Gap in Silicene by Oxidation. *ACS Nano***2014**, *8*, 10019–10025.

(13) Hu, M.; Zhang, X.; Poulikakos, D. Anomalous Thermal Response of Silicene to Uniaxial Stretching. *Phys. Rev. B***2013**, *87*, 195417.

(14) Pei, Q.; Zhang, Y.; Sha, Z.; Shenoy, V. Tuning the Thermal Conductivity of Silicene with Tensile Strain and Isotopic Doping: A Molecular Dynamics Study. *J. Appl. Phys.***2013**, *114*, 033526.

(15) Boukai, A. I.; Bunimovich, Y.; Tahir-Kheli, J.; Yu, J.; Goddard III, W. A.; Heath, J. R. Silicon Nanowires as Efficient Thermoelectric Materials. *Nature***2008**, *451*, 168–171.

(16) Hochbaum, A. I.; Chen, R.; Delgado, R.; Liang, W.; Garnett, E. C.; Najarian, M.; Majumdar, A.; Yang, P. Enhanced Thermoelectric Performance of Rough Silicon Nanowires. *Nature***2008**, *451*, 163–167.

(17) Butler, S. Z.; Hollen, S. M.; Cao, L.; Cui, Y.; Gupta, J. A.; Gutie, H. R.; Heinz, T. F.; Hong, S. S.; Huang, J.; Ismach, A. F.; *et al.* Opportunities in Two-Dimensional Materials Beyond Graphene. *ACS Nano***2013**, *7*, 2898–2926.

(18) De Padova, P.; Quaresima, C.; Ottaviani, C.; Sheverdyaeva, P. M.; Moras, P.; Carbone, C.; Topwal, D.; Olivieri, B.; Kara, A.; Oughaddou, H.; *et al.* Evidence of Graphene-like Electronic Signature in Silicene Nanoribbons. *Appl. Phys. Lett.***2010**, *96*, 261905.

(19) Zhang, X.; Xie, H.; Hu, M.; Bao, H.; Yue, S.; Qin, G.; Su, G. Thermal Conductivity of Silicene Calculated Using an Optimized Stillinger-Weber Potential. *Phys. Rev. B***2014**, *89*, 054310.

(20) Leroy, F.; Schulte, J.; Balasubramanian, G.; Böhm, M. C. Influence of Longitudinal Isotope Substitution on the Thermal Conductivity of Carbon Nanotubes: Results of Nonequilibrium Molecular Dynamics and Local Density Functional Calculations. *J. Chem. Phys.***2014**, *140*, 144704.

(21) Chen, S.; Wu, Q.; Mishra, C.; Kang, J.; Zhang, H.; Cho, K.; Cai, W.; Balandin, A. A.; Ruoff, R. S. Thermal Conductivity of Isotopically Modified Graphene. *Nat. Mater.***2012**, *11*, 203–207.

(22) Hao, F.; Fang, D.; Xu, Z. Mechanical and Thermal Transport Properties of Graphene with Defects. *Appl. Phys. Lett.***2011**, *99*, 041901.

(23) Yang, N.; Zhang, G.; Li, B. Ultra Low Thermal Conductivity of Isotope-Doped Silicon Nanowires. *Nano Lett.***2008**, *8*, 276–280.

(24) Broderick, S.; Ray, U.; Srinivasan, S.; Rajan, K.; Balasubramanian, G. An Informatics Based Analysis of the Impact of Isotope Substitution on Phonon Modes in Graphene. *Appl. Phys. Lett.***2014**, *104*, 243110.

(25) Ray, U.; Balasubramanian, G. Reduced Thermal Conductivity of Isotope Substituted Carbon Nanomaterials: Nanotube versus Graphene Nanoribbon. *Chem. Phys. Lett.***2014**, *599*, 154–158.

(26) Lindsay, L.; Broido, D. A.; Mingo, N. Flexural Phonons and Thermal Transport in Graphene. *Phys. Rev. B***2010**, *82*, 115427.

(27) Balasubramanian, G.; Puri, I. K.; Böhm, M. C.; Leroy, F. Thermal Conductivity Reduction through Isotope Substitution in Nanomaterials: Predictions from an Analytical Classical Model and Nonequilibrium Molecular Dynamics Simulations. *Nanoscale***2011**, *3*, 3714–3720.

(28) Liu, B.; Reddy, C. D.; Jiang, J.; Zhu, H.; Baimova, J.; Dmitriev, S. V; Zhou, K. Thermal Conductivity of Silicene Nanosheets and the Effect of Isotopic Doping. *J. Phys. D. Appl. Phys.***2014**, *47*, 165301.

(29) Tang, Q.; Zhou, Z. Graphene-Analogous Low-Dimensional Materials. *Prog. Mater. Sci.***2013**, *58*, 1244–1315.

(30) Geim, A. K.; Grigorieva, I. V. Van Der Waals Heterostructures. *Nature***2013**, *499*, 419–425.

(31) Chen, S.; Wu, Q.; Mishra, C.; Kang, J.; Zhang, H.; Cho, K.; Cai, W.; Balandin, A. A.; Ruoff, R. S. Thermal Conductivity of Isotopically Modified Graphene. *Nat. Mater.***2012**, *11*, 203–207.

(32) Zhang, G.; Li, B. Impacts of Doping on Thermal and Thermoelectric Properties of Nanomaterials. *Nanoscale***2010**, *2*, 1058.

(33) Adamyan, V.; Zavalniuk, V. Lattice Thermal Conductivity of Graphene with Conventionally Isotopic Defects. *J. Phys. Condens. Matter***2012**, *24*, 415401.

(34) Nika, D. L.; Pokatilov, E.; Balandin, A. Theoretical Description of Thermal Transport in Graphene: The Issues of Phonon Cut-off Frequencies and Polarization Branches. *Phys. Status Solidi (B).***2011**, *248*, 2609–2614.

(35) J. Tersoff. Modeling Solid-State Chemistry: Interatomic Potentials for Multicomponent Systems. *Phys. Rev. B***1989**, *39*, 5566–5568.

(36) Plimpton, S. Fast Parallel Algorithms for Short-Range Molecular Dynamics. *J. Comput. Phys.***1995**, *117*, 1–19.

(37) Humphrey, W.; Dalke, A.; Schulten, K. VMD: Visual Molecular Dynamics. *J. Mol. Graph.***1996**, *14*, 33–38.

CHAPTER 5. GENERAL CONCLUSIONS

General Discussion

In summary our atomistic simulations in Chapter 2 predict that it is the out-of-plane delocalized low-energy vibrational modes in carbon nanotubes (CNTs) and the out-of-plane flexural vibrational modes in GNR which contribute significantly to the thermal conductivity (k) change due to isotope substitution. Leaving the ballistic-diffusive regime, the relative rate change of k was found to be constant with increase in length for both these carbon nanomaterials. While the transition of vibrations towards lower wave numbers due to incorporation of isotopes in the nanostructures are very clear, the influence of mass disorder in bringing about this change in the vibrational spectra are found to be consistent across different length scales. Chapter 3 uses the informatics approach of principal component analysis to extract features from the phonon density of states spectrum and present a data driven computational framework which speeds up the thermal conductivity predictions in isotope substituted graphene without using molecular dynamics simulations. Chapter 4 concludes that silicene, a graphene-analogous low dimensional material exhibits a stark difference from graphene with respect to their heat transport mechanism due to its buckled structure which restricts the participation of atomic vibrations perpendicular to the direction of heat transfer in the energy transfer mechanism. In spite of this, silicene still shows a similar trend in the reduction of k with increasing isotope substitution with that of graphene.

Recommendations for Future Research

Many significant problems which have practical importance can be explored in future. Carbon nanotubes (CNT), being good electrical conductors, can be used as efficient thermoelectric materials, the performance of which can be improved by increasing the figure of merit (*ZT*). This *ZT* depends on Seebeck coefficient, thermal conductivity and electrical conductivity. In our study, only the reduction in thermal conductivity of CNTs due to isotope substitution have been discussed and not the other parameters. That can be a very suitable avenue in which to channelize our research in future.

The ongoing innovative studies with Graphene has instigated the possibility to computationally model similar low-dimensional (2-D) materials like MoS_2, B_2C, BC_3 and WS_2 which can also have immensely technologically useful thermoelectric properties. A fundamental understanding of the change in thermal conductivity due to isotope substitution in all these graphene analogous 2-D materials may help us develop a scale independent computational materials property prediction paradigm for novel thermoelectrics.

APPENDIX. INPUT FILES OF LAMMPS USED FOR THE MOLECULAR DYNAMICS SIMULATIONS

Input files used

Here just the files for graphene nanoribbon is shown as an example case. All the files are in LAMMPS readable format.

Equilibration of pure graphene:

```
# Fixing NPT, NVT, NVE in GNR
dimension       3
units           metal
atom_stylemolecular
read_data    data.graphene_pure
pair_style     tersoff
pair_coeff * * SiC.tersoff  C
thermo 1
thermo_style custom step temp epair etotal press vol
minimize 1.0e-7 1.0e-9 100 10000
velocity all create 300.0 4928459
fix 1 all npt temp 300.0 300.0 0.1 iso 0.0 0.0 1
thermo 50
timestep  0.001
```

```
run 7000000

unfix 1

fix 2 all nvt temp 300.0 300.0 0.1

run 7000000

unfix 2

write_restart   equil.restart1

fix 3 all nve

dump 3 all custom 50000 dump.atomg id type x y z vx vy vz

run 2000000

write_restart    equil.restart2
```

Equilibration of 50%isotope substituted graphene sheet

```
# Fixing NPT, NVT, NVE in isotope substituted GNR

dimension     3

units          metal

atom_style molecular

read_data   data.graphenedoped50

pair_style    tersoff

pair_coeff * * SiC.tersoff  C C

variable       n index 9 ## Random 50% distribution

variable       g equal v_n-8

variable       m equal v_g*14.00

mass           1 12.0107
```

```
mass            2 $m
set             group all type/fraction 2 0.50 394812
thermo 1
thermo_style custom step temp epair etotal press vol
minimize 1.0e-7 1.0e-9 100 10000
velocity all create 300.0 4928459
fix 1 all npt temp 300.0 300.0 0.1 iso 0.0 0.0 1
thermo 50
timestep  0.001
run 7000000
unfix 1
fix 2 all nvt temp 300.0 300.0 0.1
run 7000000
unfix 2
write_restart  equil.restart1
fix 3 all nve
dump 3 all custom 50000 dump.atomg id type x y z vx vy vz
run 2000000
write_restart  equil.restart2
```

Evaluation of thermal conductivity using RNEMD

```
#Thermal Conductivity of Graphene Using Tersoff potential
read_restart    equil.restart2
pair_style    tersoff
```

```
pair_coeff * * SiC.tersoff  C C
log          log.thermal
variable     t equal 150000
thermo             $t
fix          NVT all nvt temp 300.0 300.0 0.1
compute            ke all ke/atom
variable     temperature atom c_ke/(1.5*8.617e-5)
fix     thermal all thermal/conductivity 300 x 100
thermo_style     custom step temp  pe ke etotal press lx ly lz f_thermal
run          7000000
write_restart      equil.restart3
fix          TEP all ave/spatial 1 100 100 x lower 3 v_temperature file
temp.graphenedoped50 units box
run          1000000
write_restart      equil.restart4
```

Input file for dumping velocities of the atoms used to calculate the phonon DOS

```
read_restart        equil.restart2
reset_timestep     0
log          log.vacf
pair_style      tersoff
pair_coeff      * * SiC.tersoff C C
timestep     0.001
thermo       10000
```

```
thermo_style      custom step atoms etotal pe ke temp press
fix               NVE all nve
restart           100000 vacf.restart
run               1000000
clear

label             loops
variable          s index 1 2 3 4 5 6 7 8 9 10
variable          p equal v_s*100000
read_restart      vacf.restart.$p
log               log.lammps.$s
pair_style        tersoff
pair_coeff        * * SiC.tersoff  C C
timestep          0.001
thermo            1
thermo_style      custom step atoms etotal pe ke temp press
fix               NVE all nve
dump  data all custom 1 velocities.$s.data id type mass vx vy vz
run               10000
clear
next s
jump in.velc loops
```